RSC Advances

ROYAL SOCIETY OF CHEMISTRY

www.rsc.org/advances

Surfactant effects on the synthesis of durable tin-oxide nanoparticles and its exploitation as a recyclable catalyst for elimination of toxic dye: A green and efficient approach for wastewater treatment

Archita Bhattacharjee, Md. Ahmaruzzaman* and Tanur Sinha

Department of Chemistry, National Institute of Technology Silchar, Assam- 788010, India

ABSTRACT:

A green synthesis of SnO_2 nanoparticles was developed successfully using urea by microwave heating method. This method resulted in the formation of spherical, microcrystalline SnO_2 nanoparticles with an average size of ~4.0 nm. The role of a cationic and a non-ionic surfactant, namely cetyl pyridinium chloride (CPC) and triton X-100 in the synthesis of SnO_2 nanoparticles are investigated. In this reaction, surfactants act as capping agent. Addition of surfactant along with urea leads to the formation of spherical and microcrystalline SnO_2 nanoparticles. The average particle size of the CPC assisted SnO_2 nanoparticles is ~4.5 nm, while that of triton X-100 assisted SnO_2 nanoparticles is ~5.8 nm. An increase in band gap energy is observed with a decrease in particle size because of three dimensional quantum confinement effect shown by the synthesized SnO_2 nanoparticles in their electronic spectra. The band gap energy of SnO_2 nanoparticles synthesized using urea is ~4.30eV, whereas that of CPC assisted SnO_2 nanoparticles and triton X-100 assisted SnO_2 nanoparticles are ~4.25 and ~4.15 eV, respectively. The synthesized SnO_2 nanoparticles were characterized by transmission electron microscopy (TEM), selected area electron diffraction (SAED) and Fourier transformed infrared spectroscopy (FT-IR). The optical properties were investigated using UV-visible spectroscopy. The synthesized SnO_2 nanoparticles act as an efficient photocatalyst for the degradation of rhodamine B and methyl violet 6B dye under direct sunlight. For the first time, Methyl Violet 6B and Rhodamine B dye were degraded by solar irradiation using SnO_2 nanoparticles as a catalyst.

Keywords: SnO_2-nanoparticles, microwave-heating, photocatalyst, degradation, methyl violet 6B, rhodamine B.

E-mail: md_a2002@rediffmail.com ; telephone/fax number: +913842-242915/+913842-224797

1. INTRODUCTION

The pollution of air and water caused by various organic contaminants leads to serious environmental problems. Dyes constitute a major class of organic compound having huge applications in our daily life. Most of the dyes are toxic but are used in textile industries, dyeing, printing, cosmetics etc. The effluents coming out from these industries contaminate water system thereby causing water pollution. This poses a threat to water bodies and our ecosystem. Hence, complete removal of dye from industrial waste water is vital for reducing water pollution. In this study, rhodamine B (RhB) and methyl violet 6B (MV6B) dyes are chosen. Rhodamine B (RhB) is a water soluble dye, used as a laser dye, colorant in textile industries, food stuff, and fluorescent water tracer. It is suspected to be carcinogenic and also causes irritation to eyes, skin and respiratory tract if swallowed by human beings and animals. Methyl violet 6B is a water soluble dye, used in textile industries, paper dyeing, paints, and printing ink. In biomedical field, MV6B is the active ingredient in gram's stain for bacterial classification. MV6B is also used as a disinfectant and is found very poisonous to animals. MV6B is carcinogenic in nature. Therefore, both RhB and MV6B dye causes adverse health effects and are real threat to human, animal and aquatic life. Numerous efforts have been devoted for the removal of dyes from industrial waste water. The search for effective means of reducing water pollution is a big challenge to many researchers. The conventional method such as adsorption of dye on activated carbon is inadequate for the treatment of dye waste water. Adsorption is a non-destructive method which transfers dye from one substance to another and give rise to a new kind of pollution which requires a further treatment [1]. In contrast, photocatalytic treatment of dye using solar or UV irradiation in presence of a suitable photocatalyst is a green technique and proves to be an effective method for the degradation of dye. This method converts dye molecule into non-toxic compounds. In this respect, nanostructural semiconductor metal oxides, being inexpensive and stable, acts as an excellent photocatalyst in the degradation of dye and proves to be an efficient method for the reduction of water pollution [2]. Several metal oxide semiconductors, such as SnO_2, TiO_2, ZnO, NiO, V_2O_5, etc have been used as

photocatalysts for the degradation of organic pollutants in water [2-7]. Among them, SnO_2 is known to be one of the most effective photocatalyst because of its high surface reactivity, large number of active sites and high absorption power of light radiation [2].

Tin oxide (SnO_2) is an n-type semiconductor with a wide band gap of 3.6 eV [8]. SnO_2 with a rutile crystal structure, is the most intensively explored metal oxide due to its potential applications in catalysis, gas sensors, dye-based solar cells, transparent conducting electrodes, rechargeable lithium batteries, etc. [9-16]. Numerous synthetic methods have been developed for the synthesis of SnO_2 nanostructures, such as sol-gel, homogeneous precipitation, microwave heating method, hydrothermal method, etc [17-20]. The cost for the preparation of SnO_2 nanoparticles in industrial scale is a challenging job in the production of material. Hence, it is very important to design a synthetic method using cheap and non-toxic reagents. The size, morphology, stability and properties of synthesized SnO_2 nanoparticles are of great importance and should be taken into consideration.

In this paper, we report a green synthesis of SnO_2 nanoparticles by microwave heating method. Among various methods, microwave heating method is chosen because of its several advantages over others, such as short reaction time, good control over particle size and uniform nucleation of powders in suspension. Herein, we develop a microwave heating method using urea which is a versatile reagent. The use of urea may lead to an enhancement of properties and morphology of SnO_2 nanoparticles.

This communication also illustrates a new surfactant-mediated method to prepare nanocrystalline SnO_2 powders. Surfactants are widely used and have wide range of applications due to their remarkable ability to influence the properties of surfaces and interfaces. The most accepted classification of surfactants is based on their dissociation in water; anionic surfactants, cationic surfactants and nonionic surfactants. Surfactants have a major role in shape-controlled synthesis of nanoparticles. Both hydrophobic and hydrophilic groups are present in surfactants. These groups effectively prevent the agglomeration of the particles and control their morphology. Surfactant molecules have also been used as capping agents [21]. The surfactant molecules anchored on the

surface of nanoparticles act as hybrid building blocks for conversion into higher-order structures [22]. The surfactant not only provides favorable site for the growth of the particulate assemblies, it also influences the formation process, including nucleation, growth, coagulation and flocculation. The surfactant mediated method applied herein provides a promising preparative approach to tin oxide nanoparticles. In this case, we introduce a cationic (cetyl pyridinium chloride, CPC) and a non-ionic surfactant (triton X-100) along with urea to investigate their role in the synthesis of SnO_2 nanoparticles. The effect of surfactants on the size and morphology of SnO_2 nanoparticles are also studied. To the best knowledge of the authors, synthesis of SnO_2 nanoparticles using $SnCl_2.2H_2O$ and urea along with CPC and triton X-100 has not been reported in the literature.

In this paper, we report the photocatalytic activity of synthesized SnO_2 nanoparticles for the photodegradation of rhodamine B and methyl violet 6B dyes under direct sunlight. In this case, for the first time, direct sunlight is used for the photodegradation of methyl violet 6B and rhodamine B dye in presence of SnO_2 nanocatalyst. Photodegradation of dye by solar irradiation is a comparatively greener approach than that with UV-light. To the best knowledge of the authors, methyl violet 6B dye is degraded for the first time using SnO_2 photocatalyst.

2. EXPERIMENTAL

2.1. Materials:

The reagents, stannous chloride dihydrate ($SnCl_2.2H_2O$), urea, cetyl pyridinium chloride, triton X-100, methyl violet 6B and rhodamine B were of analytical grade (AR) and purchased from Sigma-Aldrich. These reagents are used without further purification. Double distilled water is used for the synthesis of SnO_2 nanoparticles. All the reactions were carried out in a domestic microwave oven of 300 W.

2.2. Synthesis of SnO_2 nanoparticles:

2.2.1. Synthesis of SnO_2 nanoparticles using urea (S1):

For the synthesis of SnO_2 nanoparticles, 0.01M $SnCl_2.2H_20$ was treated with 100ml aqueous solution of 0.01M urea. The mixture was then kept in a microwave oven and irradiated with thirty

10s 300W shots. A white precipitate was formed. The obtained precipitate was centrifuged and washed several times with double distilled water. The final white product was dried at 70°C and collected for characterization. The sample is marked as S1.

2.2.2. Synthesis of SnO_2 nanoparticles using urea and cetyl pyridinium chloride (S2):

The synthesis of SnO_2 nanoparticles were carried out by treating 0.01M $SnCl_2.2H_20$ with 100ml aqueous solution of 0.01M urea. A 10 ml aqueous solution of 60mmole cetyl pyridinium chloride (cationic surfactant) was added dropwise with constant stirring. The mixture was then kept in a microwave oven and irradiated with thirty 10s 300W shots. A white precipitate was formed. The obtained white precipitate was centrifuged and washed several times with double distilled water. The final white product was dried at 70°C and collected for characterization. The sample is marked as S2.

2.2.3. Synthesis of SnO_2 nanoparticles using urea and triton X-100 (S3):

Likewise, SnO_2 nanoparticles were also synthesized by treating 0.01M $SnCl_2.2H_20$ with 100ml aqueous solution of 0.01M urea and then 10ml of 10% Triton X-100 (non-ionic surfactant) solution was added dropwise with constant stirring. The mixture was then kept in a microwave oven and irradiated with thirty 10s 300W shots. A white precipitate was obtained and marked as S3. The obtained white precipitate was centrifuged and washed several times with double distilled water. The final white product was dried at 70°C and collected for characterization.

2.3. Characterization of SnO_2 nanoparticles:

SnO_2 nanoparticles were characterized by powder X-ray diffraction (XRD) method using Phillips X'Pert PRO diffractometer with CuKα radiation of wavelength 1.5418Å. The size, morphology and diffraction ring pattern of SnO_2 nanoparticles were determined by JEM-2100 Transmission Electron Microscope. Infrared spectra were recorded in the wave number range from 400 to 4000cm^{-1} by using Bruker Hyperion 3000 FTIR spectrometer. UV-visible absorption spectra of the synthesized SnO_2 nanoparticles were recorded on Cary 100 BIO UV-visible spectrophotometer equipped with 1cm quartz cell.

2.4. Photocatalytic activity of synthesized SnO_2 nanoparticles:

The photocatalytic activity of SnO_2 nanoparticles (S1) were evaluated by the degradation of methyl violet 6B (MV6B) and rhodamine B (RhB) under direct sunlight. To evaluate the photocatalytic activity, 10 mg of SnO_2 photocatalyst (S1) was dispersed in 200ml of 10^{-4}M aqueous solution of two different dyes by sonication. These dyes were then exposed to sunlight irradiation. The experiments were carried out on a sunny day (23rd May 2014) at Silchar city between 10 a.m–3 p.m (outside temperature 35^0- 40^0C). At a regular interval of time, 4ml of the two different suspensions were withdrawn and centrifuged immediately. The progress of the reaction was monitored by taking UV-visible spectroscopy at a regular interval of time.

3. RESULTS AND DISCUSSION

3.1. FT-IR studies:

Fig. 1(a, b and c) represents the FT-IR spectra of the synthesized S1, S2 and S3 nanoparticles respectively. The assignment of FT-IR bands of synthesized SnO_2 nanoparticles (S1, S2 and S3) are summarized in Table 1. The band observed around 3439- 3442 cm^{-1} is due to –OH vibration of water adsorbed on the surface of SnO_2 nanoparticles. The presence of water is also confirmed by a sharp peak at 1629 cm^{-1} which is due to H_2O deformation. The peak around 610-600 cm^{-1} is assigned to Sn-O-Sn stretching mode of surface bridging oxide formed by the condensation of adjacent surface hydroxyl groups [17, 23, 9, 4].

FT-IR spectra is recorded not only to detect the formation of SnO_2 nanoparticles but also to perceive the existence of capping agents (CPC and triton X-100) adsorbed on the surface of SnO_2 nanoparticles. In the synthesis of S2 nanoparticles, CPC is used as a capping agent. FT-IR spectra of S2 nanoparticles show bands in the region 3000-3100 cm^{-1} due to N-H stretching which indicates that some molecules of CPC are adsorbed on the surface of SnO_2 nanoparticles along with traces of urea. The presence of alkyl chain is indicated by the peak around 2919 cm^{-1} and 2850 cm^{-1} which are due to asymmetric and symmetric C-H stretch, respectively. This further confirms the presence of CPC on the surface of SnO_2 nanoparticles as a capping agent.

The FT-IR spectra of S3 nanoparticle is represented in Fig. 1(c). In the synthesis of S3 nanoparticles, the surfactant triton X-100 is used as a surface capping agent. The band observed around 3439 cm^{-1} is assigned to –OH vibration of triton X-100 along with water adsorbed on the surface of SnO_2 nanoparticles. The peak around 1248 cm^{-1} and 1114 cm^{-1} is due to asymmetric and symmetric C-O stretching of triton X-100, respectively. The bands around 2942 cm^{-1} and 2876 cm^{-1} indicates the presence of alkyl chain. This confirms that some molecules of triton X-100 are adsorbed on the surface of SnO_2 nanoparticles. Hence, from the FT-IR spectra it is evident that surfactant CPC and triton X-100 are adsorbed on the surface of SnO_2 nanoparticles and thereby acts as a good capping agent.

[Position for Table 1]

3.2. XRD studies:

Fig. 2 represents the XRD patterns of the synthesized SnO_2 nanoparticles (S1, S2, and S3). The XRD pattern of synthesized S1 nanoparticles (Fig. 2a) shows peak at 2θ values of 26.8 ^{o}, 34.06 ^{o}, 38.02 ^{o}, 52.01 ^{o}, 54.9 ^{o}, 58.1 ^{o}, 62.02 ^{o}, 64.9 ^{o}, 66.03 ^{o} , 71.6 ^{o} and 79.1 ^{o} which corresponds to the (1 1 0), (1 0 1), (2 0 0), (2 1 1), (2 2 0), (0 0 2), (3 1 0), (1 1 2), (3 0 1), (2 0 2) and (3 2 1) plane, respectively. All peaks are well indexed to the tetragonal rutile structure of SnO_2 nanoparticles (JCPDS 41-1445) [24, 25].

The synthesized SnO_2 nanoparticles (S2) (Fig. 2b) shows diffraction peak at 2θ= 26.8 ^{o}, 34.1 ^{o}, 38.2 ^{o}, 52.01 ^{o}, 55.05 ^{o}, 58.2 ^{o}, 62.1 ^{o}, 64.9 ^{o}, 66.3 ^{o}, 71.6 ^{o} and 78.9 ^{o} which corresponds to (1 1 0), (1 0 1), (2 0 0), (2 1 1), (2 2 0), (0 0 2), (3 1 0), (1 1 2), (3 0 1), (2 0 2) and (3 2 1) plane, respectively. The obtained peak positions are in excellent agreement with the tetragonal rutile structure of SnO_2 nanoparticles (JCPDS 41-1445) [24, 25].

The XRD pattern of SnO_2 nanoparticles (S3) (Fig. 2c) shows diffraction peaks at 2θ= 26.9 ^{o}, 34.3 ^{o}, 38.1 ^{o}, 52.03 ^{o}, 55.07 ^{o}, 58.4 ^{o}, 62.3 ^{o}, 65.09 ^{o}, 66.09 ^{o}, 71.5 ^{o} and 78.8 ^{o} which corresponds to the lattice plane (1 1 0), (1 0 1), (2 0 0), (2 1 1), (2 2 0), (0 0 2), (3 1 0), (1 1 2), (3 0 1), (2 0 2) and (3 2

1) respectively. All peaks are well indexed to the tetragonal rutile structure of SnO_2 nanoparticles (JCPDS 41-1445) [24, 25].

Hence, the XRD data (Fig. 2) confirms the formation of SnO_2 nanoparticles possessing a tetragonal rutile crystal structure. The average crystallite size of synthesized SnO_2 nanoparticles can be calculated from the XRD data using Debye-Scherrer equation [24, 25]:

$$D = \frac{k\lambda}{\beta \cos\theta} \qquad \text{---------} \ (1)$$

where D is the crystallite size, λ is the X-ray wavelength, β is the full width at half maximum (FWHM) of the diffraction peak, θ is the Bragg diffraction angle and k is the so-called shape factor whose value is about 0.9. The average crystallite size of S1, S2 and S3 nanoparticles calculated using equation (1) are 4.2, 4.8 and 6.0 nm respectively.

Hence, it is evident that the grain size of SnO_2 nanoparticles increased when surfactants are introduced as capping agents. The particle size of SnO_2 nanoparticles formed using non-ionic surfactant (triton X-100) is greater than that formed using cationic surfactant (CPC). Hence, from the above studies it is evident that the size of SnO_2 nanoparticles can be tuned by introducing surfactants as capping agents.

3.3. TEM and SAED studies:

The morphology and the size distribution of synthesized SnO_2 nanoparticles (S1) can be depicted from the TEM images (Fig. 3a) and from SAED pattern (Fig. 3d). The microstructure of the nanoparticles is examined by the high resolution transmission electron microscopy (HRTEM). Fig. 3 (c) shows the HRTEM image of the SnO_2 nanoparticles (S1). From the TEM image (Fig. 3a) it is evident that spherical SnO_2 nanoparticles are formed with an average particle size of ~4.0 nm. Interestingly, a clock like structure is observed in the domain of spherical SnO_2 nanoparticles (Fig. 3b). The lattice spacing is calculated from the HRTEM image (Fig. 3c) and found to be 0.23 nm which corresponds to (200) lattice plane. The SAED pattern (Fig. 3d) indicates the micro-crystalline structure of SnO_2 nanoparticles. The lattice spacings are calculated from Fig. 3(d) and found to be

0.32 nm, 0.25 nm and 0.17 nm which correspond to the lattice plane (110), (101) and (211), respectively. The observed lattice planes are in excellent agreement with the reported tetragonal rutile structure of SnO_2 nanoparticles [24, 25].

Fig. 4(a) and 4(c) shows the TEM image and SAED pattern of SnO_2 nanoparticles formed using urea and cetyl pyridinium chloride (CPC). The microstructure of the nanoparticles is investigated by the HRTEM images (Fig. 4b). Fig. 4(a) shows the formation of spherical SnO_2 nanoparticles with an average particle size of ~4.5 nm. The lattice spacing calculated from the HRTEM image (Fig. 4b) is found to be 0.17 nm which corresponds to (211) lattice plane. The SAED pattern (Fig. 4c) shows diffused concentric rings and reveal the microcrystalline nature of the SnO_2 nanoparticles. The diffusion is preferably due to the attachment of the surfactant at the surface of nanoparticles. The lattice spacing are found to be 0.34 nm, 0.26 nm, 0.22 nm and 0.17 nm and corresponds to the lattice plane (110), (101), (200) and (211), respectively. The lattice planes obtained from the SAED pattern are in good agreement with the reported tetragonal rutile structure of SnO_2 nanoparticles [24, 25].

The morphology and the size distribution of SnO_2 nanoparticles formed using urea and triton X-100 can be depicted from the TEM images (Fig. 5a) and from SAED pattern (Fig. 5c). Fig. 5(b) shows the HRTEM images of the SnO_2 nanoparticles. TEM image (fig. 5a) depicts the formation of spherical SnO_2 nanoparticles with an average particle size of about ~5.8 nm. The lattice spacing calculated from the HRTEM image (Fig. 5b) is found to be 0.21 nm and 0.17 nm which correspond to (200) and (211) lattice plane. The SAED pattern (Fig. 5c) shows concentric diffraction rings which reveal the microcrystalline nature of the SnO_2 nanoparticles. The lattice spacing are observed to be 0.33 nm, 0.25 nm, 0.23 nm and 0.17 nm which corresponds to the lattice plane (110), (101), (200) and (211), respectively. The obtained lattice plane depicts the tetragonal rutile structure of SnO_2 nanoparticles [24, 25].

Hence, from the TEM images and SAED pattern it is confirmed that SnO_2 nanoparticles are formed using urea with various surfactants. The results obtained from TEM images and SAED pattern are

in excellent agreement with the XRD data. The surface modification of SnO_2 nanoparticles is achieved by the introduction of cationic and non-ionic surfactant, namely CPC and triton X-100 respectively. The synthesized SnO_2 nanoparticles are spherical and microcrystalline in nature. The average particle size of SnO_2 nanoparticles formed using urea is about 4.0 nm whereas the average particle size of CPC assisted SnO_2 nanoparticles is about 4.5 nm and that of triton X-100 assisted SnO_2 nanoparticles is about 5.8 nm. Hence, it is evident that the grain size of SnO_2 nanoparticles increased when surfactants are introduced as capping agents. The particle size of SnO_2 nanoparticles formed using non-ionic surfactant (triton X-100) is greater than that of SnO_2 nanoparticles formed using cationic surfactant (CPC). This may be attributed to the fact that the surfactants which are used in the synthesis formed miceller encapsulation of different size and shape. Accordingly, the size and shape of the nanoparticles will be influenced by that of the micelle formed.

3.4. Optical properties:

Semiconductor nanoparticles showed a three dimensional quantum size effect in their electronic spectra. It was observed that the band gap energy increases with a decrease in particle size and the absorption edge shows a blue shift. Fig. 6(a) shows the absorption spectra of synthesized SnO_2 nanoparticles (S1). From the UV-vis spectra, it is apparent that the absorption onset is about 285 nm. The absorption spectra of CPC assisted SnO_2 nanoparticles (S2) is represented in Fig. 7(a) and the absorption onset is about 290 nm. Fig. 8(a) represents the UV-visible spectra of Triton X-100 assisted SnO_2 nanoparticles (S3). The absorption onset is about 296 nm. Hence, the absorption edge shows a red shift with an increase in the particle size. This indicates that the particles are in quantum regime.

The band gap energy (E_g) of the SnO_2 nanoparticles can be calculated from the absorption spectra using Tauc plot. For semiconductor nanoparticles following equation have been used to relate absorption coefficient with incident photon energy

$$\alpha(\nu)\, h\nu = K\,(h\nu - E_g)^n \quad \text{---------- (2)}$$

where E_g is the band gap energy, hν is the incident photon energy, K is a constant, α(ν) is absorption coefficient which can be defined by the Beer-Lambert's law as follows:

α(ν) = 2.303Aρ/cl, where A is the absorbance, ρ is the density of the SnO_2 nanoparticles, c is the concentration and l is the path length. The exponent 'n' in equation (2) depends on the type of the transition and n may have values ½, 2, 3/2, 3 for allowed direct, allowed indirect, forbidden direct and forbidden indirect transitions respectively. In case of SnO_2 nanoparticles the value of n is ½ for allowed direct transition. Therefore, by plotting $(\alpha h\nu)^2$ versus hν and by extrapolating the curve to zero absorption coefficient band gap (E_g) can be determined using equation (2) [26].

Fig. 6(b), 7(b), and 8(b) represents the plot of $(\alpha h\nu)^2$ versus photon energy (hν) for S1, S2 and S3 nanoparticles, respectively. By extrapolating the curve to zero absorption co-efficient, band gap energy can be calculated using equation (1). The intercept of the tangent to the plot provides a good estimation of the band gap energy. The band gap energy of SnO_2 nanoparticles synthesized using urea (S1) is 4.30 eV. The band gap energy of CPC assisted SnO_2 nanoparticles (S2) and triton X-100 assisted SnO_2 nanoparticles (S3) are found to be 4.25 eV and 4.15 eV, respectively.

In case of semiconductors, band gap energy depends on the particle size. From the Fig. 6(b), 7(b) and 8(b), it is evident that the band gap energy decreases with an increase in grain size of the SnO_2 nanoparticles and the absorption edge shows a red shift. This is due to three dimensional quantum confinement effects which occur in semiconductor nanoparticles. Hence, the synthesized SnO_2 nanoparticles are in the quantum regime. The band gap energy of the synthesized SnO_2 nanoparticles is larger than the band gap energy of bulk SnO_2 (3.6 eV). The selective growth of crystal and distinct morphology (clock like structure) may influence more significant blue shift of the band gap.

Table 2 summarizes the result obtained from FT-IR, XRD, TEM and UV-visible spectra for the synthesized SnO_2 nanoparticles (S1, S2 and S3). The bands in the FT-IR spectra confirm that the surfactant molecules act as capping agents in the formation of SnO_2 nanoparticles. Interestingly, the average particle size of synthesized SnO_2 nanoparticle is found to increase by the introduction of

cationic and non-ionic surfactant molecules which are acting as capping agents. The grain size of SnO_2 nanoparticles synthesized using triton X-100 (non-ionic surfactant) is greater than that obtained using CPC (cationic surfactant). This may be due to the fact that the surfactants used in the synthesis form miceller encapsulation of various size and shape. Accordingly, the size and shape of the nanoparticles will be influenced by that of the miceller structure formed. From the TEM images it is evident that the synthesized SnO_2 nanoparticles (S1, S2 and S3) are spherical in nature. The band gap energy of synthesized SnO_2 nanoparticles showed a clear blue shift from 4.15 to 4.30 eV with a decrease in particle size from 5.8 to 4.0 nm. This is due to a three dimensional quantum confinement effect shown by the synthesized SnO_2 nanoparticles.

[Position for Table 2]

3.5. Reaction mechanism for the synthesis of SnO_2 nanoparticles:

The most plausible mechanism for the synthesis of SnO_2 nanoparticles can be visualized as follows: On microwave heating, urea will decompose to give ammonium hydroxide and carbon dioxide. The produced ammonium hydroxide then reacts with the precursor molecule, $SnCl_2.2H_20$ to form a white precipitate of tin hydroxide, $Sn(OH)_2$. This on further microwave heating decomposes to give tin oxide (SnO_2) nanoparticles.

Step I:

$$H_2N-\overset{\overset{\displaystyle O}{\|}}{C}-NH_2 + H_2O \longrightarrow NH_4OH + CO_2$$

Step II:

$$SnCl_2.2H_2O + NH_4OH \longrightarrow Sn(OH)_2$$

Step III:

$$Sn(OH)_2 \longrightarrow SnO_2$$

3.6. Role of cationic and non-ionic surfactant in the synthesis of SnO_2 nanoparticles:

The formation of particle is a very complex process. It involves nucleation, growth, coagulation and flocculation, which are influenced considerably by the surfactant assemblies [27]. The addition of surfactants viz., CPC and Triton X-100 can affect the nucleation during the oxides crystallization process. After nucleation, surfactant can influence particle growth, coagulation and flocculation. Therefore, surfactant plays an important role in the preparation of metal oxides nanoparticles.

The cationic surfactant, CPC is used as a capping agent in the synthesis of SnO_2 nanoparticles (S2). This method is based on the chelation of cations (metal) by surfactant in an aqueous solution. On microwave irradiation, urea is attacked by strong nucleophilic nitrogen atoms of cetylpyridinium chloride (CPC) molecules, which leads to the weakening of C=O double bonds in the structure of urea and forms transitional product, urea-cetylpyridinium chlorine (UCPC). At an appropriate temperature, the C=O bond will break, and O^{2-} anion will gradually generate, which then reacts with Sn^{2+} to form SnO_2 nanoparticles. With the formation of SnO_2 nanoparticles, the ligand (UCPC) interacts with them and caps effectively most of the surface of SnO_2 nanoparticles [28].

The synthesis of S3 nanoparticles were carried out in presence of a non-ionic surfactant, triton X-100. This method involves selective adsorption of surfactant molecules on the surfaces of the SnO_2 nanoparticles. The hydrophobic interactions between the surfactant molecules on adjacent nanoparticles are responsible for bringing together the obtained inorganic–organic hybrid building blocks. The reaction was carried out in aqueous solution. During the reaction, hydrophilic poly(ethylene oxide) (PEO) chains of Triton X-100 were immersed into water cores with the hydrophobic heads left outside. This leads to the formation of SnO_2 nanocrytals. The repulsion of the outer hydrophobic heads protected the nanoparticles from further aggregation [29].

3.7. Evaluation of photocatalytic activity of synthesized SnO_2 nanoparticles:

Two different dyes, namely rhodamine B and methyl violet 6B were chosen for evaluating the photocatalytic activity of SnO_2 nanoparticles. These dyes have different chromophoric groups and

selected from two different categories. Rhodamine B is a heteropolyatomic dye and methyl violet 6B is a triphenyl methane dye.

The photocatalytic activity of SnO_2 nanoparticles (S1) were examined by adding 10mg of the photocatalyst to 200ml of 10^{-4}M aqueous solution of each dye. The degradation of the dye does not take place immediately when irradiated with sunlight. The degradation process involves photochemical reactions on the surface of the SnO_2 nanoparticles. Hence an increase in the surface area of the photocatalyst leads to the greater degradation of the dye. The size and the dispersion of the photocatalyst in the solution plays an important role in the degradation of dye.

The photocatalytic activity of SnO_2 nanoparticles were examined by monitoring the changes in the absorption spectra of RhB and MV6B dye solution during their photodegradation process. Fig. 9(a) shows the absorption spectra of photocatalytic degradation of RhB dye using SnO_2 nanoparticles under direct sunlight. The UV-visible spectra of the dye (RhB) shows a strong absorption band around 553nm and the addition of SnO_2 nanoparticles leads to a decrease of the absorption band with time. It is observed that the intensity of the peaks gradually decreases with an increase in irradiation time. After completion of 3h, the solution becomes colorless. The absorption band at 553nm disappears indicating the complete decomposition of the dye. Fig. 10(a) represents the UV-visible spectra for the photocatalytic degradation of MV6B dye by sunlight irradiation. From the spectra it is evident that MV6B shows a strong absorption band around 580 nm which decreases gradually with irradiation time after the addition of SnO_2 nanoparticles. After 3h, the solution becomes colorless and the absorption band at 580nm disappears, indicating the complete destruction of the chromophoric structure of the dye. Degradation of dye is a pseudo-first order reaction and its kinetics may be expressed as follows [30]:

$$\ln (C_o/C) = kt \qquad \text{---------- (3)}$$

where k is the rate constant, C_o and C are the absorbance or concentration before and after degradation of dye, respectively.

The rate constant for the photodegradation of RhB and MV6B dye can be calculated using equation (3). Fig. 9(b) and 10(b) represents the plot of $\ln(C_o/C)$ versus irradiation time (t) for RhB and MV6B dye. The plot gives a linear relationship. Hence, the slope of the line represents the rate constant (k) for the photodegradation of RhB and MV6B dye. The value of k is found to be 1.76×10^{-2} min^{-1} and 1.72×10^{-2} min^{-1} for RhB and MV6B dye, respectively.

The percentage efficiency of photodegradation of the dye was determined using the following equation [31]:

$$X = [(C_o - C)/C] \times 100 \quad \text{---------- (4)}$$

Fig. 9(c) shows graphically the percentage efficiency of photocatalytic degradation of RhB dye with time. It was observed that 99.01% of the dye degraded photochemically within 240 min under direct sunlight using SnO_2 nanoparticles. Fig. 10(c) represents the percentage efficiency of photocatalytic degradation of MV6B dye with time. It was evident that 98.3% of MV6B dye degraded photochemically within 240 min by solar irradiation using SnO_2 nanoparticles.

3.8. Mechanism of photodegradation of RhB and MV6B using SnO_2 nanoparticles:

When the surface of SnO_2 nano catalyst is irradiated with energy greater than its band-gap energy, it leads to the formation of holes (h^+) in the valence band and an electron (e^-) in the conduction band of SnO_2 nanoparticles. The holes (h^+) act as an oxidizing agent and oxidized the pollutant directly or react with water to form hydroxyl radicals. The electron (e^-) in the conduction band acts as a reducing agent and reduces the oxygen adsorbed on the SnO_2 nanocatalyst.

The plausible mechanism for the photocatalytic degradation of RhB can be schematically visualized as [9]:

$$SnO_2 + h\nu \rightarrow e^- + h^+$$

$$H_2O + h^+ \rightarrow OH^- + H^+$$

$$OH^- + h^+ \rightarrow {}^{\bullet}OH$$

$$e^- + O_2 \rightarrow {}^{\bullet}O_2^-$$

$${}^{\bullet}O_2^- + H^+ \rightarrow {}^{\bullet}OOH$$

$$RhB + h\nu \rightarrow RhB^*$$

$$RhB^* + SnO_2 \rightarrow RhB + SnO_2\ (e^-)$$

$$SnO_2\ (e^-) + O_2 \rightarrow SnO_2 + O_2^-$$

$$SnO_2\ (e^-) + {}^{\bullet}O_2^- + H^+ \rightarrow SnO_2 + H_2O_2$$

$$SnO_2\ (e^-) + H_2O_2 \rightarrow SnO_2 + {}^{\bullet}OH + OH^-$$

$$h^+ + RhB \rightarrow \text{degradation products}$$

$$RhB^* + O_2 \text{ or } {}^{\bullet}OH \text{ or } {}^{\bullet}O_2^- \rightarrow \text{degradation products}$$

The probable degrdadation mechanism of MV6B on SnO_2 nanocrystal may be visualized as follows:

$$SnO_2 + h\nu \rightarrow e^- + h^+$$

$$H_2O + h^+ \rightarrow OH^- + H^+$$

$$OH^- + h^+ \rightarrow {}^{\bullet}OH$$

$$e^- + O_2 \rightarrow {}^{\bullet}O_2^-$$

$${}^{\bullet}O_2^- + H^+ \rightarrow {}^{\bullet}OOH$$

$$MV6B + h\nu \rightarrow MV6B^*$$

$$MV6B^* + SnO_2 \rightarrow MV6B + SnO_2\ (e^-)$$

$$SnO_2\ (e^-) + O_2 \rightarrow SnO_2 + O_2^-$$

$$SnO_2\ (e^-) + {}^{\bullet}O_2^- + H^+ \rightarrow SnO_2 + H_2O_2$$

$$SnO_2\ (e^-) + H_2O_2 \rightarrow SnO_2 + {}^{\bullet}OH + OH^-$$

$$h^+ + MV6B \rightarrow \text{degradation products}$$

$$MV6B^* + O_2 \text{ or } {}^{\bullet}OH \text{ or } {}^{\bullet}O_2^- \rightarrow \text{degradation products}$$

The excited dye injects an electron to the conduction band of SnO_2, from which it is scavenged by pre-adsorbed oxygen, O_2, to form active oxygen radicals. These active radicals drive the photodegradation process. SnO_2 nanoparticles plays a significant role as an electron carrier. Such assisted photo processes provide an attractive route to treat dye pollutants using sunlight.

The schematic representation of the photodegradation of Rhodamine B and Methyl Violet 6B dyes using SnO_2 NPs is depicted as follows:

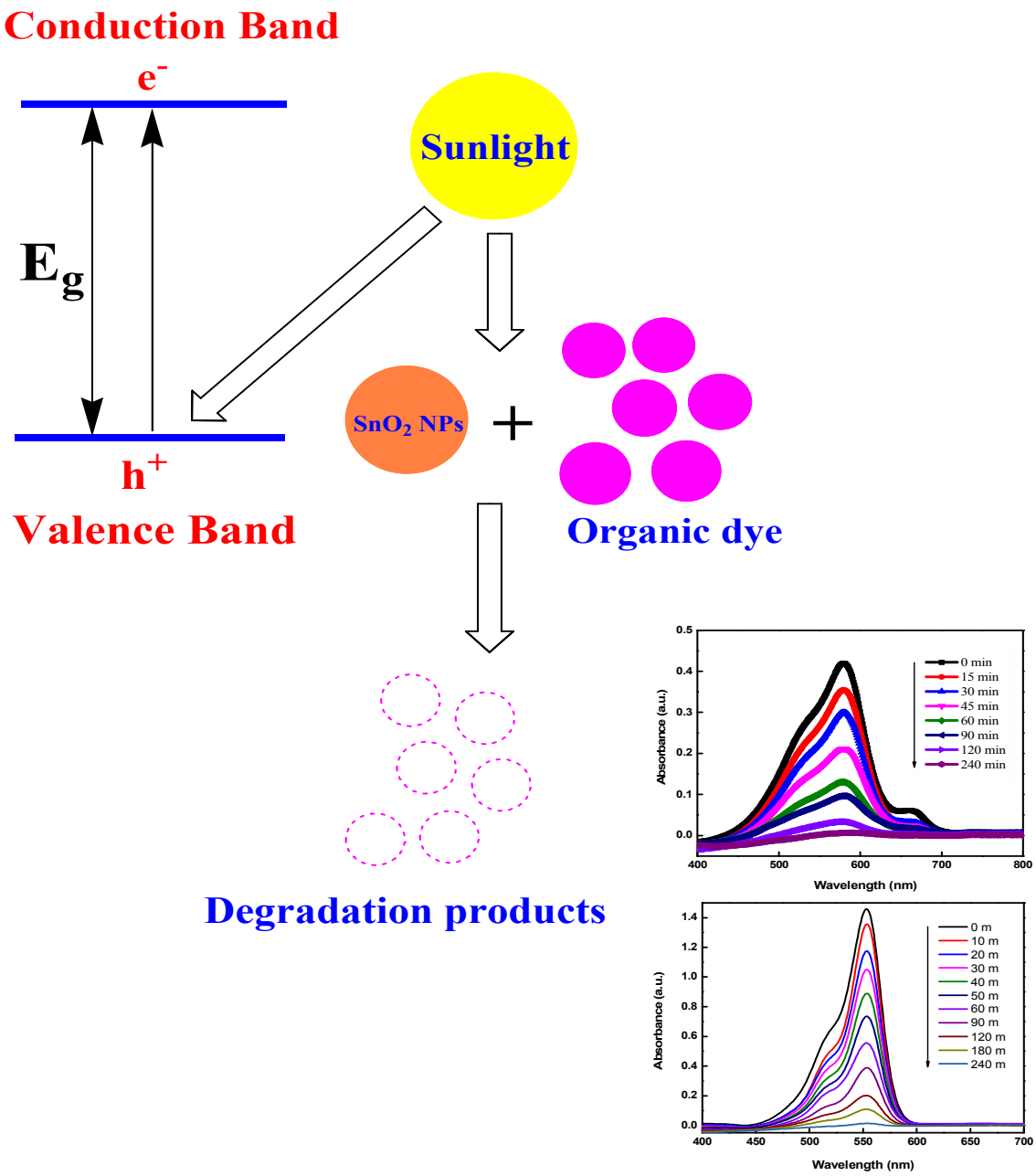

Scheme 1. Schematic representation of the photodegradation process of Rhodamine B and Methyl Violet 6B dye using SnO_2 NPs.

4. CONCLUSION

In this paper, we report a facile, green approach towards the synthesis of SnO_2 nanoparticles. A microwave heating method was developed for the synthesis of SnO_2 nanoparticles using urea. The synthesized SnO_2 nanoparticles were characterized by FT-IR, XRD, TEM, SAED and UV-visible

spectroscopy. From the TEM images and SAED pattern, it is evident that the synthesized SnO_2 nanoparticles are spherical and microcrystalline in nature with a tetragonal rutile crystalline structure. The average particle size is about 4.0 nm. The role of surfactant CPC and triton X-100 in the synthesis of SnO_2 nanoparticles was also studied. It was evident that CPC and triton X-100 acts as a capping agent. The introduction of surfactants with urea leads to an increase in the particle size of SnO_2 nanoparticles. From the TEM images and SAED pattern it is apparent that CPC and triton X-100 assisted SnO_2 nanoparticles are spherical, considerably monodispersed and microcrystalline in nature with an average size of ~4.5 nm and ~5.8 nm, respectively. The particle size obtained from the TEM images are also in good agreement with that obtained from XRD pattern. Hence, it is apparent that the particle size increases by the introduction of capping agents. This may be attributed to the fact that the surfactants which are used in the synthesis form miceller encapsulation of different size and shape. Accordingly, the size and shape of the nanoparticles are influenced by that of the miceller structure formed by the surfactant molecules. The synthesized SnO_2 nanoparticles showed a three dimensional quantum confinement effect. Therefore the band gap energy of synthesized SnO_2 nanoparticles shows a clear blue shift from 4.15 to 4.30 eV with a decrease in particle size from 5.8 nm-4.0 nm. Thus, from the above studies it can be stated that the size of the SnO_2 nanoparticles can be tuned by introducing surfactants as capping agents. The synthesized SnO_2 nanoparticles act as an efficient photocatalyst for the degradation rhodamine B and methyl violet 6B under direct sunlight.

Acknowledgement

We, the authors, express our heartfelt thanks and gratitude to the Director, NIT Silchar and TEQIP-II for providing lab facilities and scholarship. Our special thanks are extended to NEHU, IIT Bombay and Gauhati University for providing TEM, IR and XRD data.

References:

1. J. Pal, M. K. Deb, D. K. Deshmukh, B. K. Sen, *Appl. Nanosci.,* 2014, **4,** 61-65

2. G. Sangami, N. Dharmaraj, *Spectrochim. Acta. A. Mol. Biomol. Spectrosc.,* 2012, **97,** 847-852

3. A. L. Linsebigler, G. Lu, J. T. Yates, *Chem. Rev.,* 1995, **95,** 735−758

4. W. Jianga, J. A. Joens, D. D. Dionysioub, K. E. O'Shea, *J. Photochem. Photobiol. A: Chem.,* 2013, **262,** 7-13

5. H. Qin, W. Li, Y. Xia, T. He, *ACS Appl. Mater. Interfaces,* 2011, **3,** 3152−3156

6. L. Liu, Y. Li, S. M. Yuan, M. Ge, M. M. Ren, C. S. Sun, Z. Zhou, *J. Phys. Chem. C,* 2010, **114,** 251−255

7. C. J. Mao, H. C. Pan, X. C. Wu, J. J. Zhu, H. Y. Chen, *J. Phys. Chem. B,* 2006, **110,** 14709−14713

8. S. C. Yeow, W. L. Ong, A. S. W. Wong, G. W. Ho, *Sens. Actuators B,* 2009, **143,** 295-301

9. S. K. Kansal, M. Singh, D. Sud, *J. Hazard. Mater.,* 2007, **141,** 581-590

10. S. Wu, H. Cao, S. Yin, X. Liu, X. Zhang, *J. Phys. Chem. C,* 2009, **113,** 17893–17898

11. N. Srivastava, M. Mukhopadhyay, *Ind. Eng. Chem. Res.,* dx.doi.org/10.1021/ie5020052

12. N. L. V. Carreno, H. V. Fajardo, A. P. Maciel, A. Valentini, F. M. Pontes, L. F. D. Probst, E. R. Leite, E. Longo, *J. Mol. Catal. A: Chem.,* 2004, **207,** 91-96

13. F. Li, J. Xu, X. Yu, L. Chen, J. Zhu, Z. Yang, X. Xin, *Sens. Actuators B,* 2002, **81,** 165- 169

14. G. Shang, J. Wu, M. Huang, J. Lin, Z. Lan, Y. Huang, L. Fan, *J. Phys. Chem. C,* 2012, **116,** 20140-20145

15. Y. S. He, J. C. Campbell, R. C. Murphy, M. F. Arendt, J. S. Swinnea, *J. Mater. Res.,* 1993, **8,** 3131-3134

16. J. Li, Y. Zhao, N. Wang, L. Guan, *Chem. Commun.,* 2011, **47,** 5238-5240

17. J. Zhang, L. Gao, *J. Solid State Chem.,* 2004, **177,** 1425-1430.

18. K. C. Song, Y. Kang, *Mater. Lett.,* 2002, **42,** 283-289.

19. J. -J. Zhu, J. -M. Zhu, X. -H. Liao, J. -L. Fang, M. -G. Zhou, H. -Y. Chen, *Mater. Lett.,* 2002, **53,** 12-19.

20. H. -C. Chiu, C. S. Yeh, *J. Phys. Chem. C,* 2007, **111,** 7256-7259.

21. S. M. Lee, Y. Jun, S. N. Cho, J. Cheon, *J. Am. Chem. Soc.,* 2002, **124,** 11244-11245

22. M. Li, H. Schnablegger, S. Mann, *Nature,* 1999, **402,** 393-395

23. F. Gu, S. F. Wang, C. F. Song, M. K. Lü, Y. X. Qi, G. J. Zhou, D. Xu, D. R. Yuan, *Chem. Phys. Lett.,* 2003, **372,** 451-454

24. G. E. Patil, D. D. Kajale, V. B. Gaikwad, G. H. Jain, *Int. Nano Lett.,* 2012, **2,** 17-21.

25. A. Bhattacharjee, M. Ahmaruzzaman, A.K. Sil, T. Sinha, *J. Ind. Eng. Chem.* (2014), http://dx.doi.org/10.1016/j.jiec.2014.07.001

26. F. Gu, S. F. Wang, M. K. Lü, G. J. Zhou, D. Xu, D. R. Yuan, *J. Phys. Chem. B,* 2004, **108,** 8119-8123.

27. S.G. Dixit, A. R. Mahadeshwar, S. K. Haram, *Colloids Surf., A,*1998, **133,** 69-75

28. D. Wang, D. Li, L. Guo, F. Fu, Z. Zhang, Q. Wei, *J. Phys. Chem. C,* 2009, **113,** 5984–5990

29. F. Luo, D. Wu, L. Gao, S. Lian, E. Wang, Z. Kang, Y. Lan, L. Xu, *J. Cryst. Growth,* 2005, **285,** 534–540

30. J. G. Yu, H. G. Yu, B. Cheng, X. J. Zhao, J. C. Yu, W. K. Ho, *J. Phys. Chem. B,* 2003, **107,** 13871-13879.

31. S. Ghasemi, S. Rahimnejad, S.R. Setayesh, S. Rohani, M.R. Gholami, *J. Hazard. Mater.,* 2009, **172,** 1573-1578

FIGURE CAPTIONS:

1. Figure 1. FT-IR spectra of synthesized SnO_2 nanoparticles (a) S1 (b) S2 and (c) S3.

2. Figure 2. XRD pattern of synthesized SnO_2 nanoparticles (a) S1 (b) S2 and (c) S3.

3. Figure 3. (a) TEM microphotograph of synthesized SnO_2 nanoparticles (S1) (b) A clock like structure observed in the domain of synthesized spherical SnO_2 nanoparticles (S1), (c) HRTEM image of synthesized SnO_2 nanoparticles (S1), (d) SAED pattern of synthesized SnO_2 nanoparticles (S1).

4. Figure 4. (a) TEM microphotograph of synthesized SnO_2 nanoparticles (S2) (b) HRTEM images synthesized SnO_2 nanoparticles (S2)**,** (c) SAED pattern of synthesized SnO_2 nanoparticles (S2)**.**

5. Figure 5. (a) TEM microphotograph of synthesized SnO_2 nanoparticles (S3), (b) HRTEM images synthesized SnO_2 nanoparticles (S3), (c) SAED pattern of synthesized SnO_2 nanoparticles (S3).

6. Figure 6. (a) Absorption spectra of synthesized SnO_2 nanoparticles (S1), (b) Plot of $(\alpha h\nu)^2$ versus incident photon energy ($h\nu$) for the synthesized SnO_2 nanoparticles (S1).

7. Figure 7. (a) Absorption spectra of synthesized SnO_2 nanoparticles (S2), (b) Plot of $(\alpha h\nu)^2$ versus incident photon energy ($h\nu$) for the synthesized SnO_2 nanoparticles (S2).

8. Figure 8. (a) Absorption spectra of synthesized SnO_2 nanoparticles (S3), (b) Plot of $(\alpha h\nu)^2$ versus incident photon energy ($h\nu$) for the synthesized SnO_2 nanoparticles (S3).

9. Figure 9. (a) Photocatalytic degradation of Rhodamine B (RhB) dye by solar irradiation using synthesized SnO_2 nanopaticles (S1) as catalyst, (b) Plot of $\ln(C_o/C)$ versus irradiation time for photodegradation of Rhodamine B (RhB) dye using synthesized SnO_2 nanoparticles, (c) Percentage efficiency of photodegradation of Rhodamine B (RhB) dye with time.

10. Figure 10. (a) Photocatalytic degradation of Methyl violet 6B (MV6B) dye by solar irradiation using synthesized SnO_2 nanopaticles (S1) as catalyst, (b) Plot of $\ln(C_o/C)$ versus irradiation time for photodegradation of Methyl violet 6B (MV6B) dye using synthesized SnO_2

nanoparticles, (c) Percentage efficiency of photodegradation of Methyl violet 6B (MV6B) dye with time.

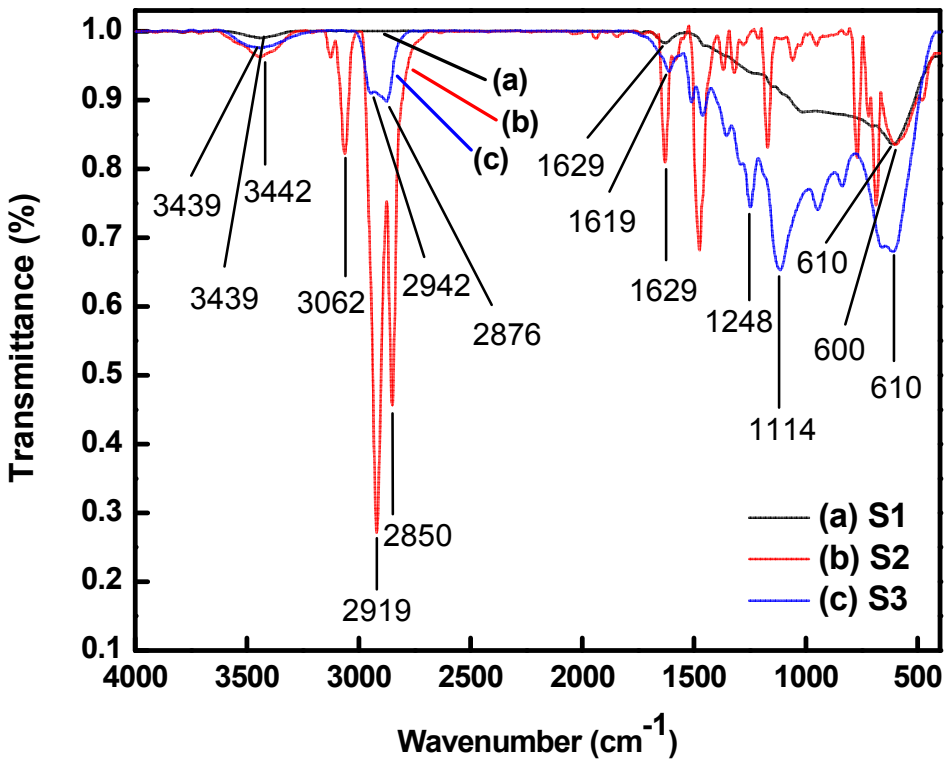

Fig. 1(a) FT-IR spectra of synthesized SnO_2 nanoparticles (S1)

Fig. 1(b) FT-IR spectra of synthesized SnO_2 nanoparticles (S2)

Fig. 1(a) FT-IR spectra of synthesized SnO_2 nanoparticles (S3)

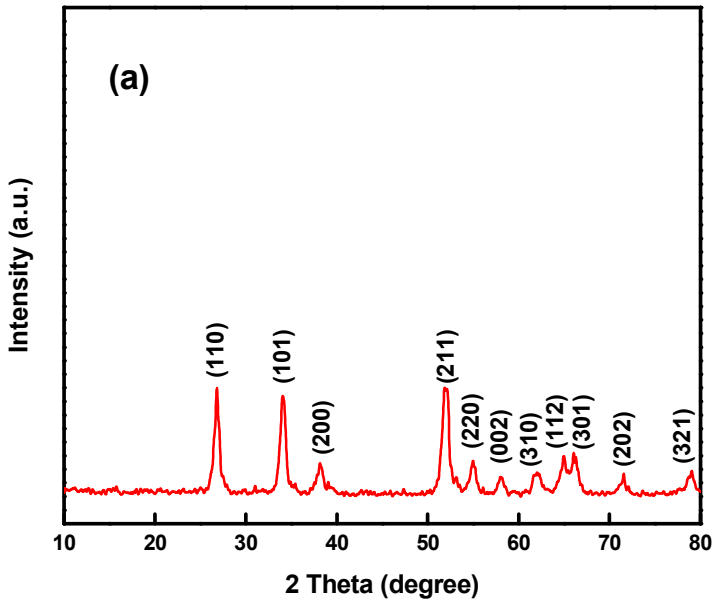

Fig. 2(a) XRD pattern of synthesized SnO_2 nanoparticles (S1)

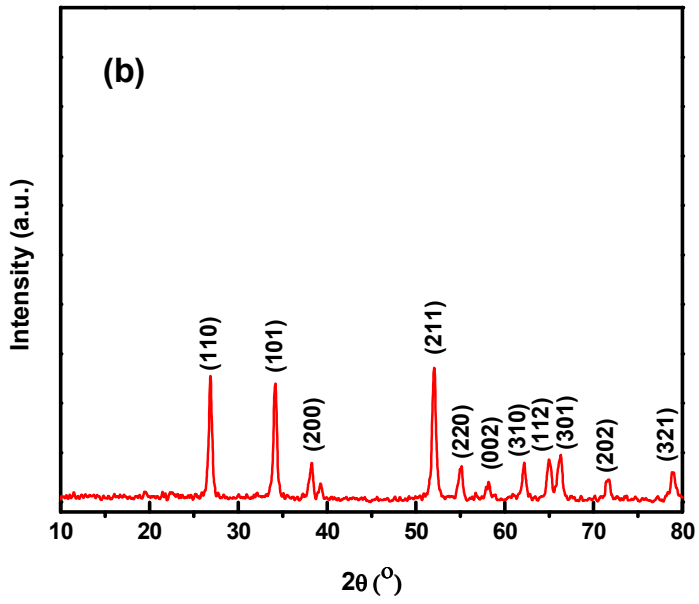

Fig. 2(b) XRD pattern of synthesized SnO_2 nanoparticles (S2)

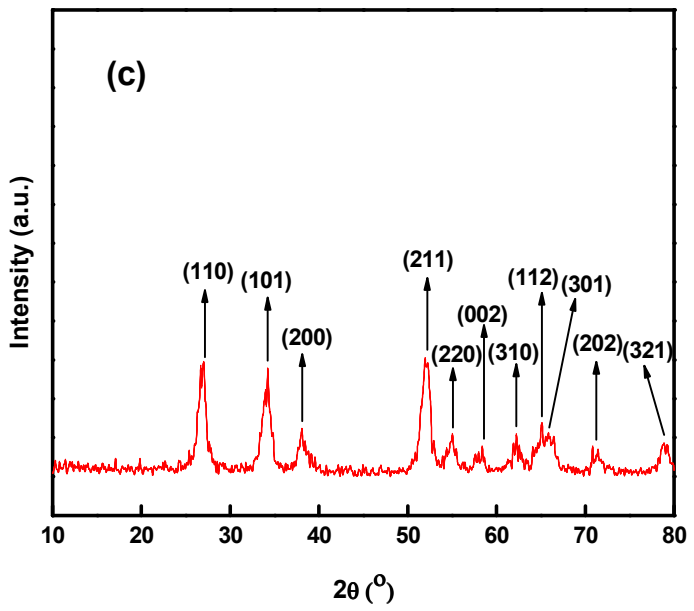

Fig. 2(c) XRD pattern of synthesized SnO_2 nanoparticles (S3)

534

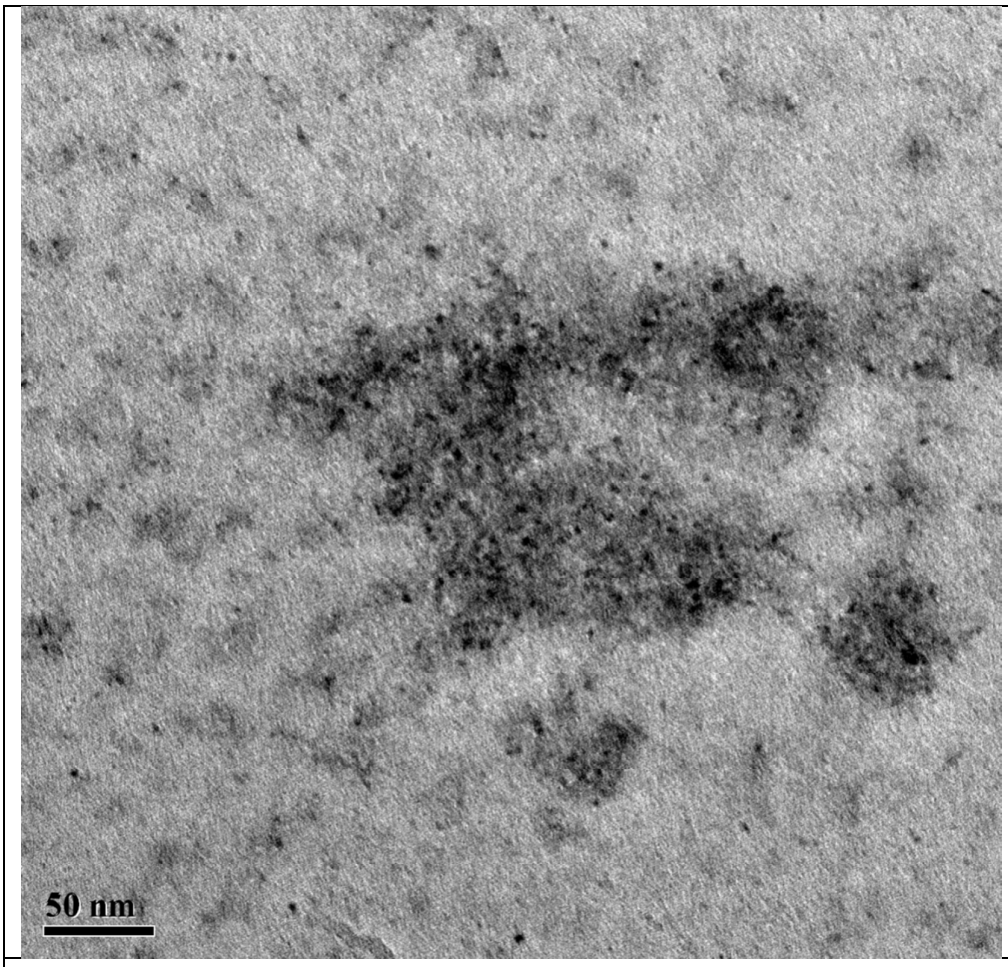

Fig. 3(a) TEM image of synthesized SnO_2 nanoparticles (S1)

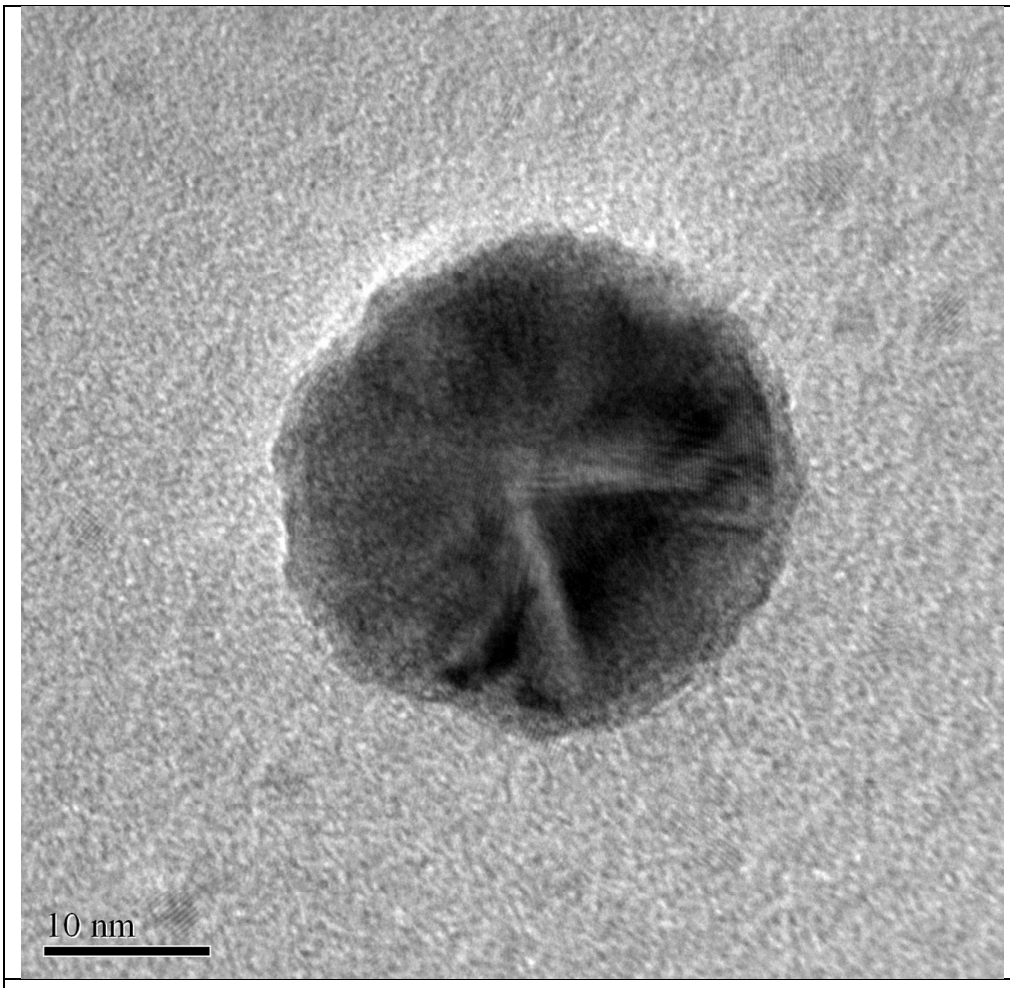

Fig. 3(b) A clock like structure in the domain of spherical SnO_2 nanoparticles (S1)

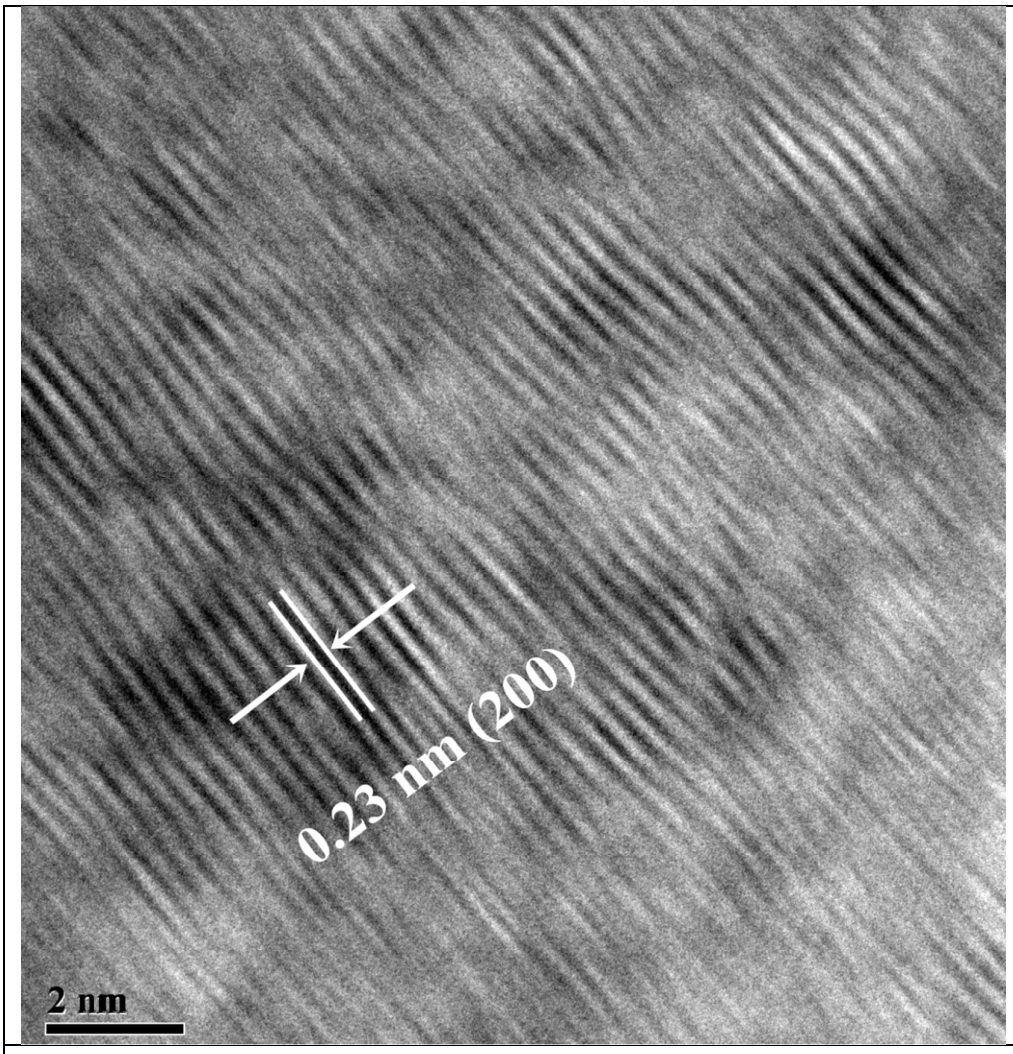

Fig. 3(c) HRTEM image of synthesized SnO_2 nanoparticles (S1)

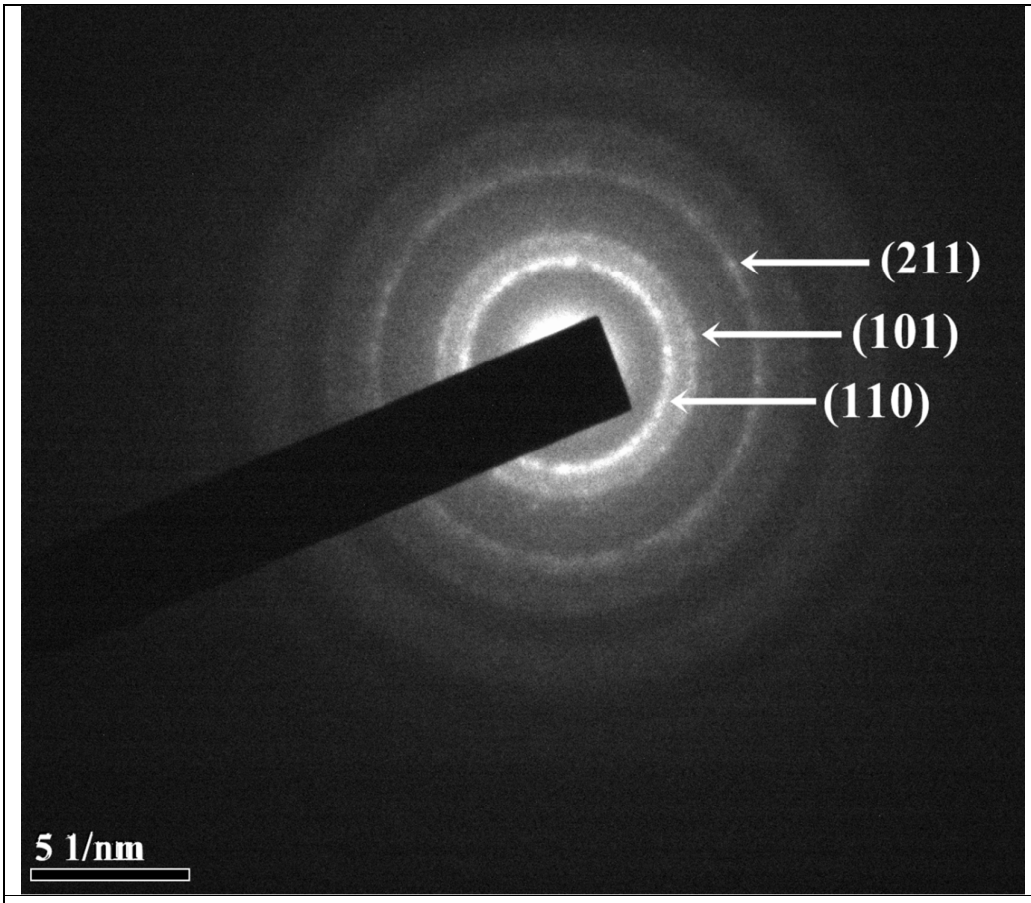

Fig. 3(d) SAED pattern of synthesized SnO_2 nanoparticles (S1)

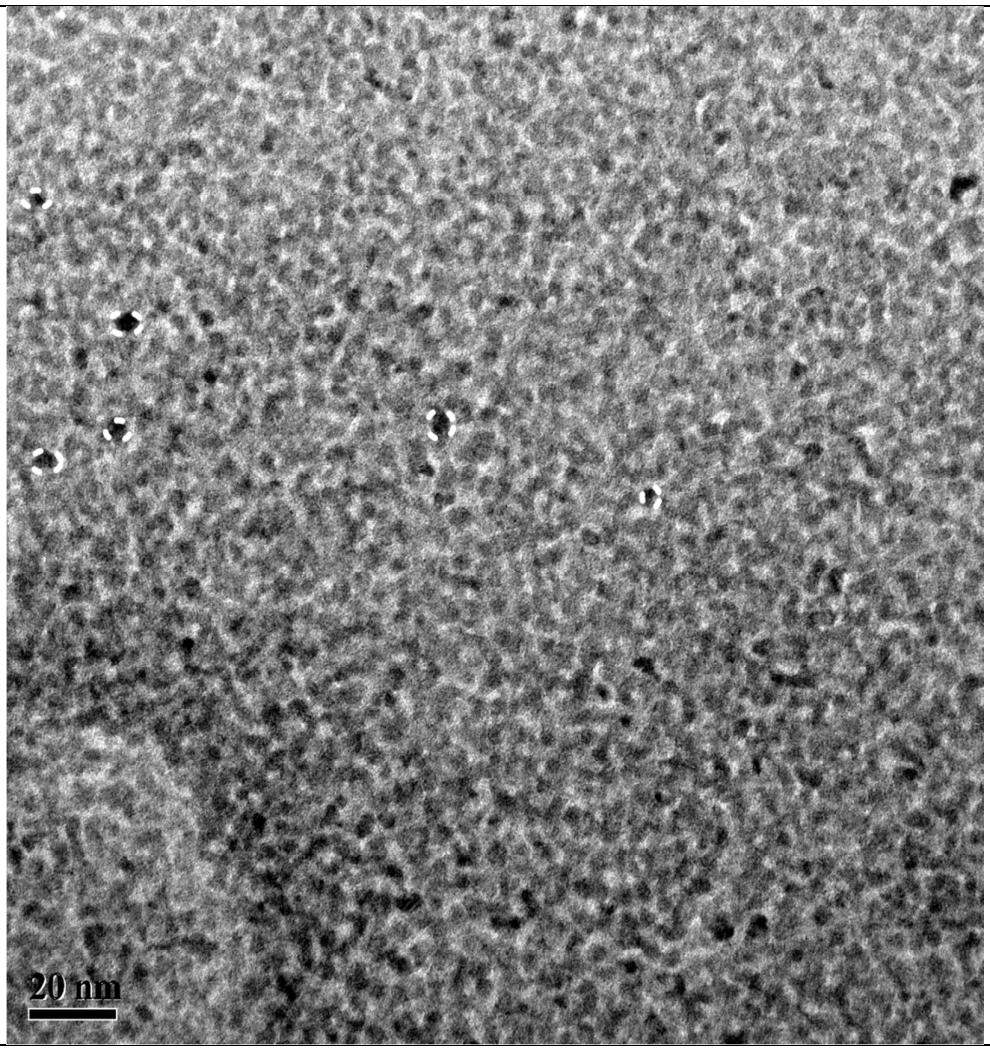

Fig. 4(a) TEM microphotograph of synthesized SnO_2 nanoparticles (S2)

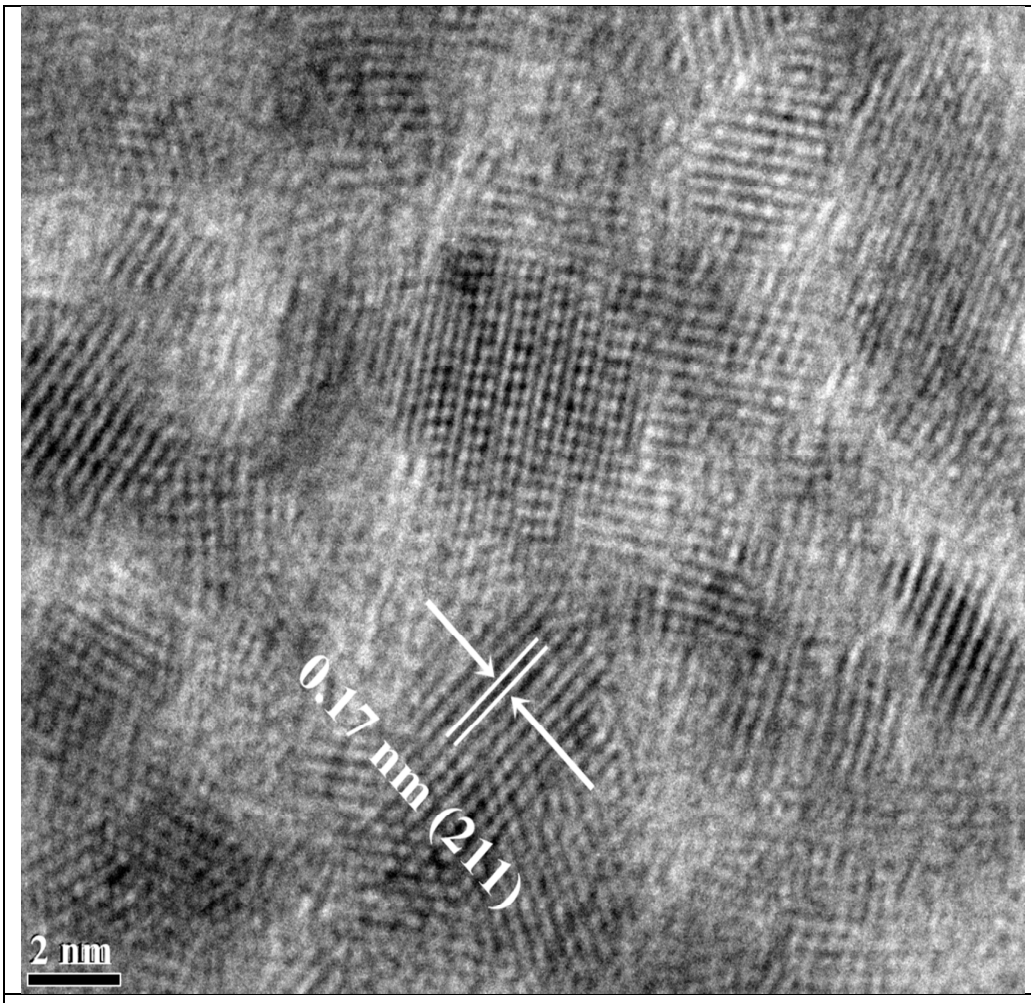

Fig. 4(b) HRTEM image of synthesized SnO_2 nanoparticles (S2)

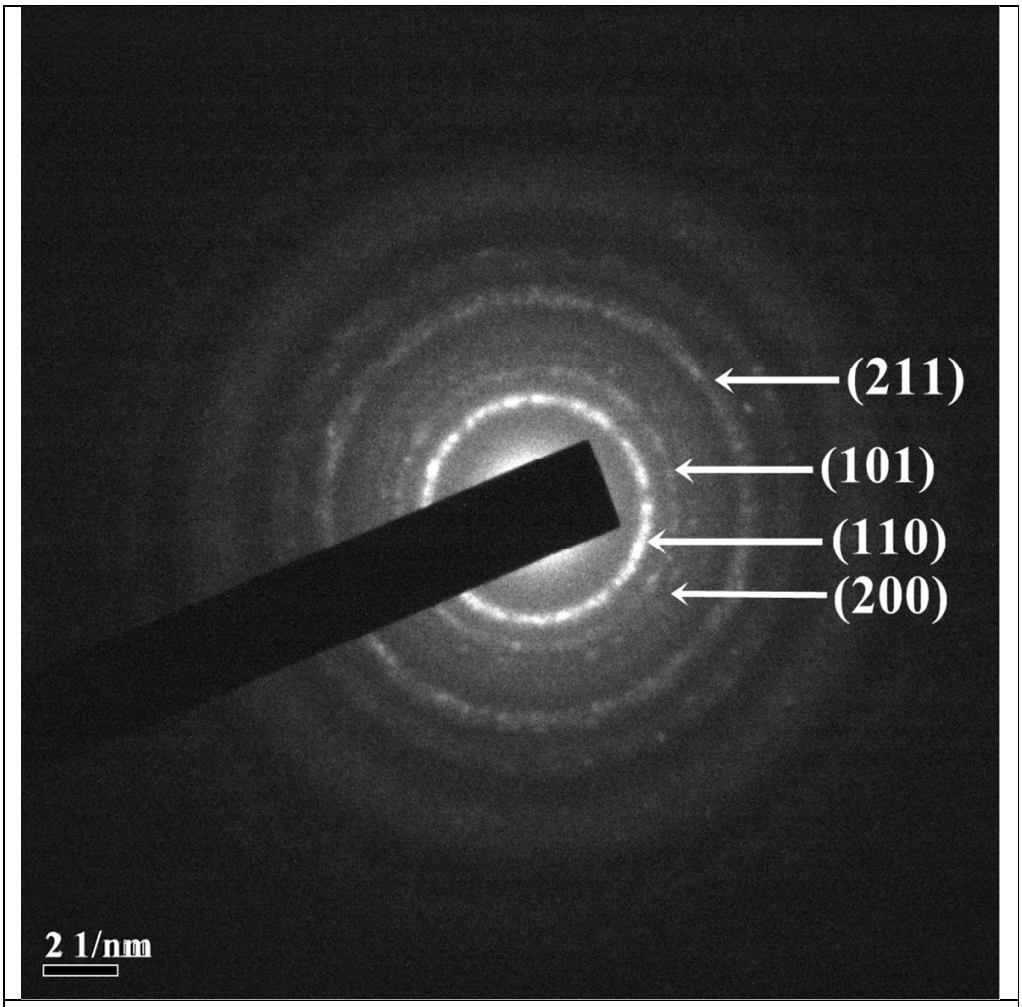

Fig. 4(c) SAED pattern of synthesized SnO_2 nanoparticles (S2)

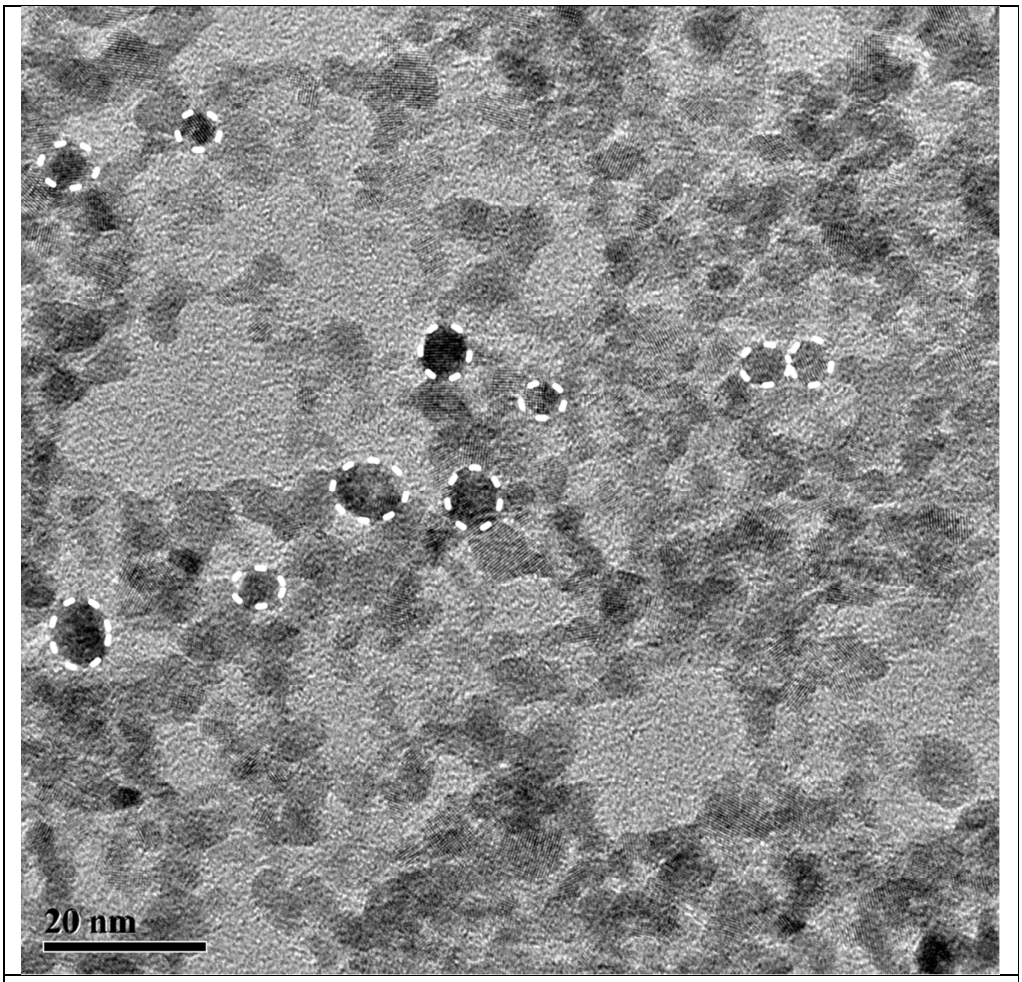

Fig. 5(a) TEM image of synthesized SnO_2 nanoparticles (S3)

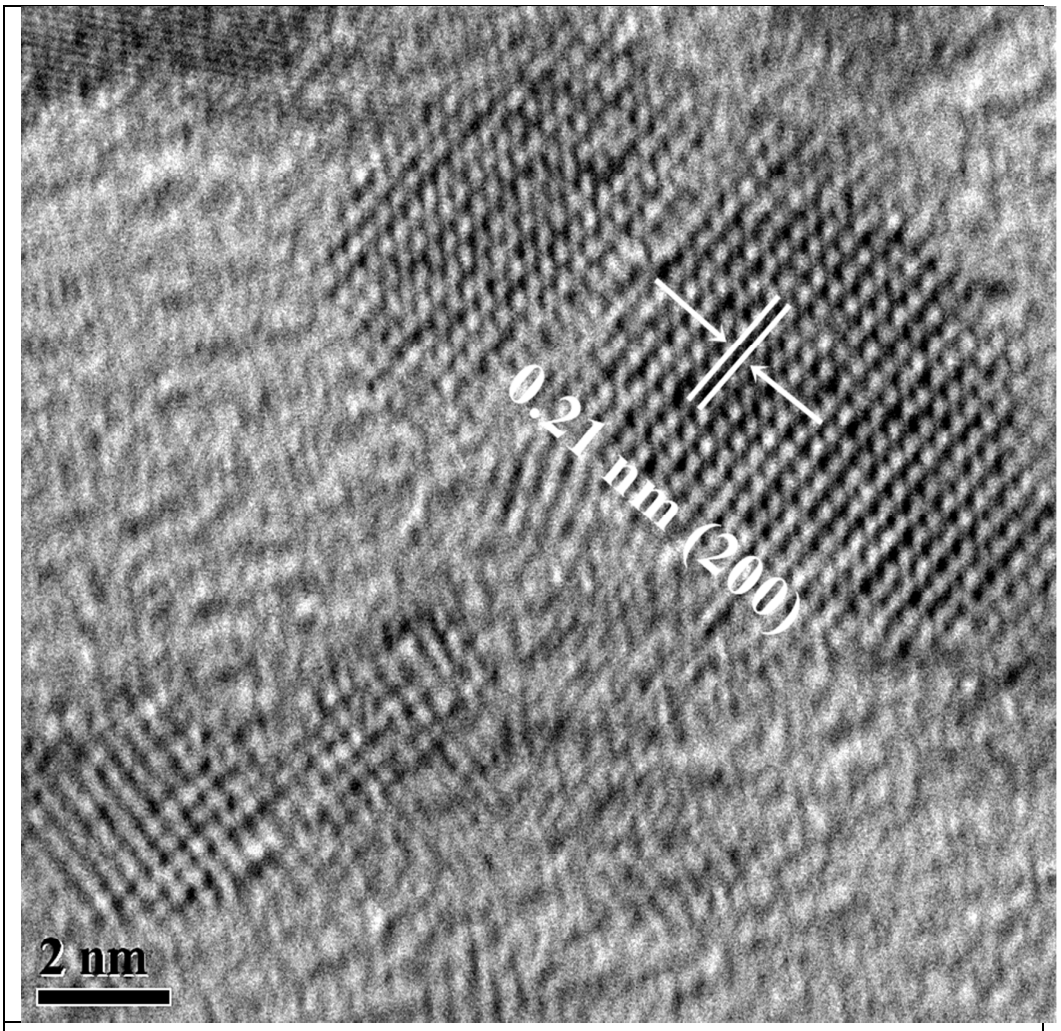

Fig. 5(b) HRTEM image of synthesized SnO_2 nanoparticles (S3)

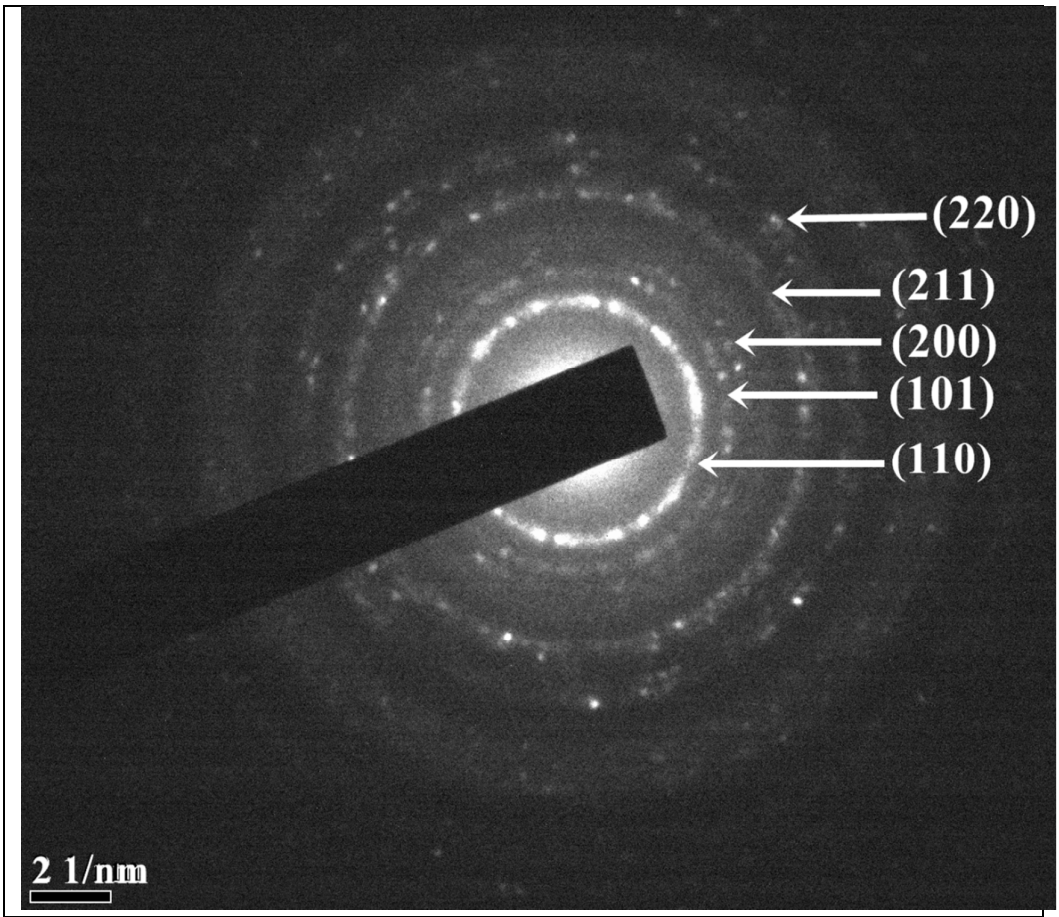

Fig. 5(c) SAED pattern of synthesized SnO_2 nanoparticles (S3)

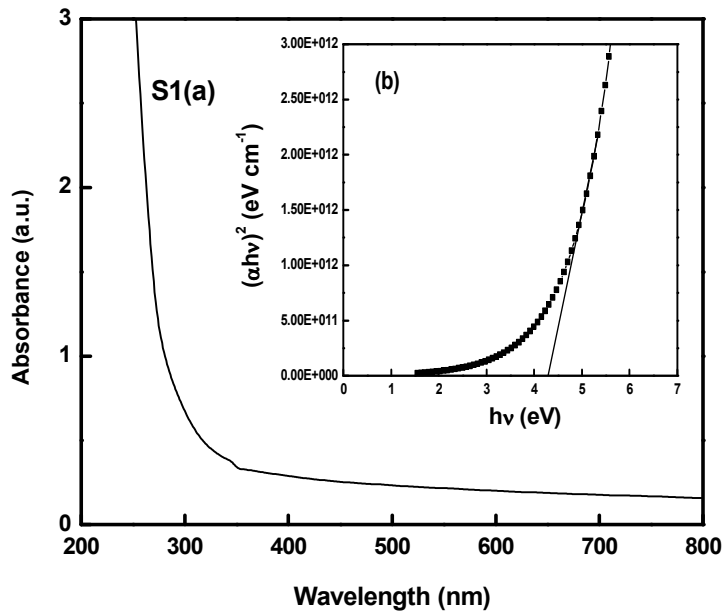

Fig. 6(a) UV-visible absorption spectra of synthesized SnO_2 nanoparticles (S1)

Fig. 6(b) Plot of $(\alpha h\nu)^2$ versus incident photon energy (hν) for the synthesized SnO_2 nanoparticles (S1)

537

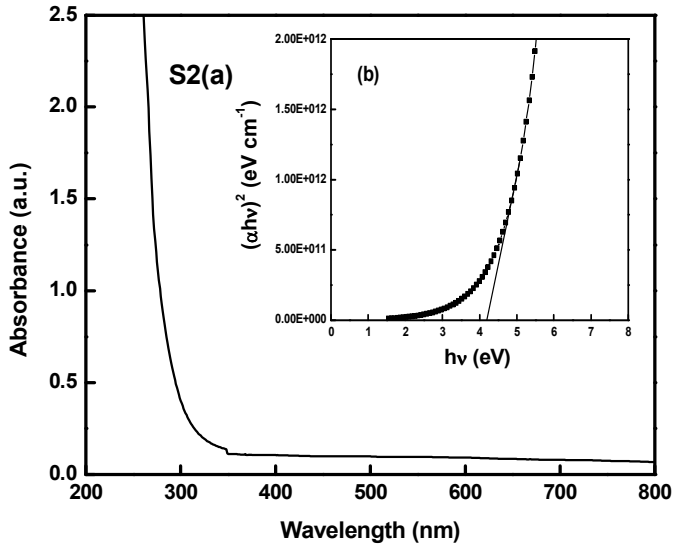

Fig. 7(a) UV-visible absorption spectra of synthesized SnO_2 nanoparticles (S2)

Fig. 7(b) Plot of $(\alpha h\nu)^2$ versus incident photon energy (hν) for the synthesized SnO_2 nanoparticles (S2)

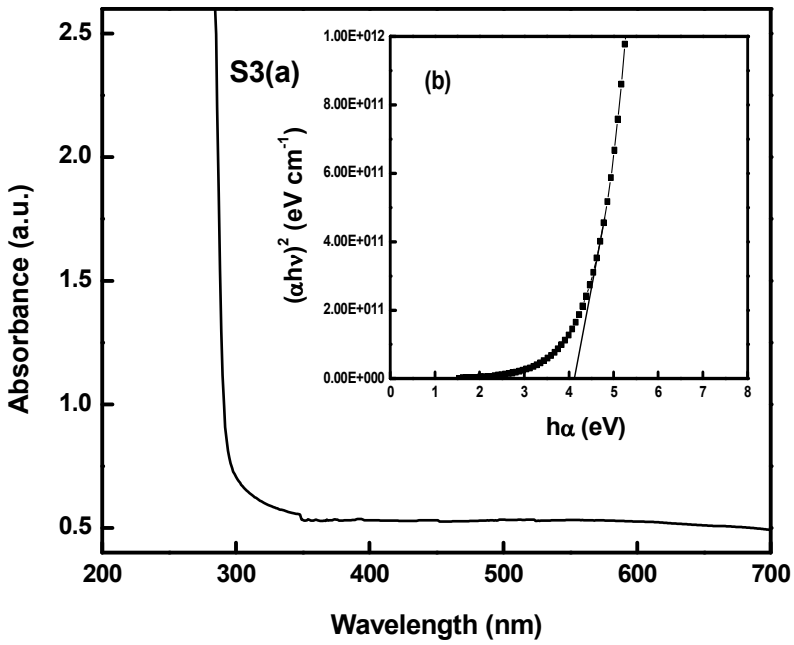

Fig. 8(a) UV-visible absorption spectra of synthesized SnO_2 nanoparticles (S3)

Fig. 8(b) Plot of $(\alpha h\nu)^2$ versus incident photon energy ($h\nu$) for the synthesized SnO_2 nanoparticles (S3)

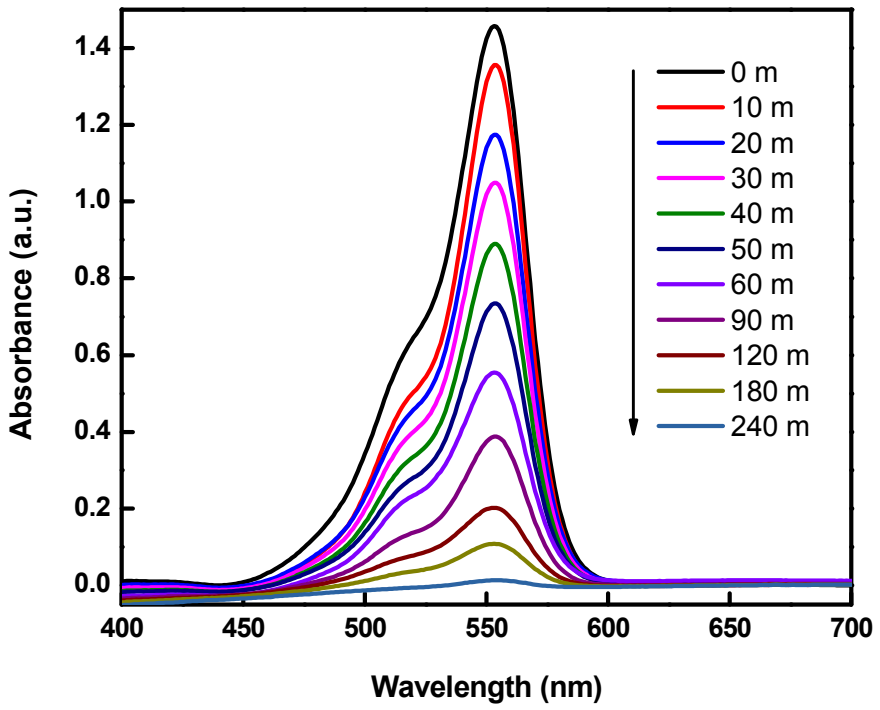

Fig. 9(a) Photocatalytic degradation of Rhodamine B (RhB) dye by solar irradiation using synthesized SnO_2 nanopaticles (S1) as catalyst.

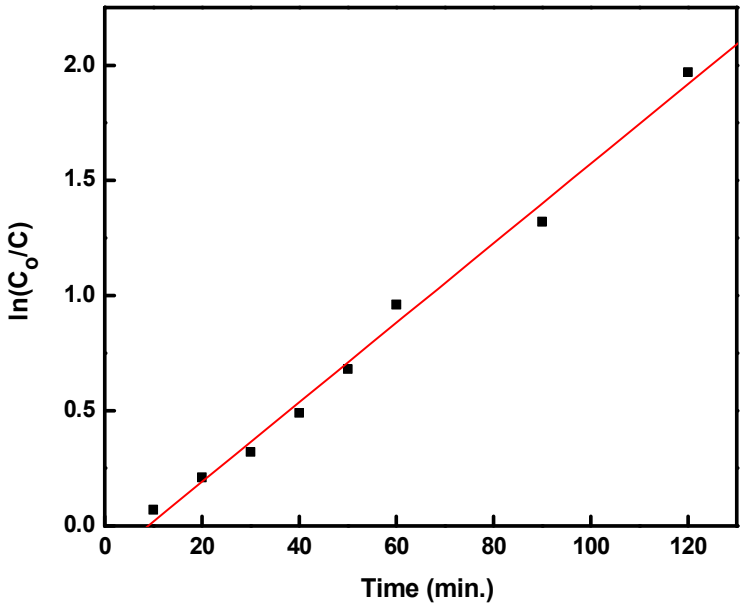

Fig. 9(b) Plot of ln(C_o/C) versus irradiation time for photodegradation of Rhodamine B (RhB) dye using synthesized SnO_2 nanoparticles.

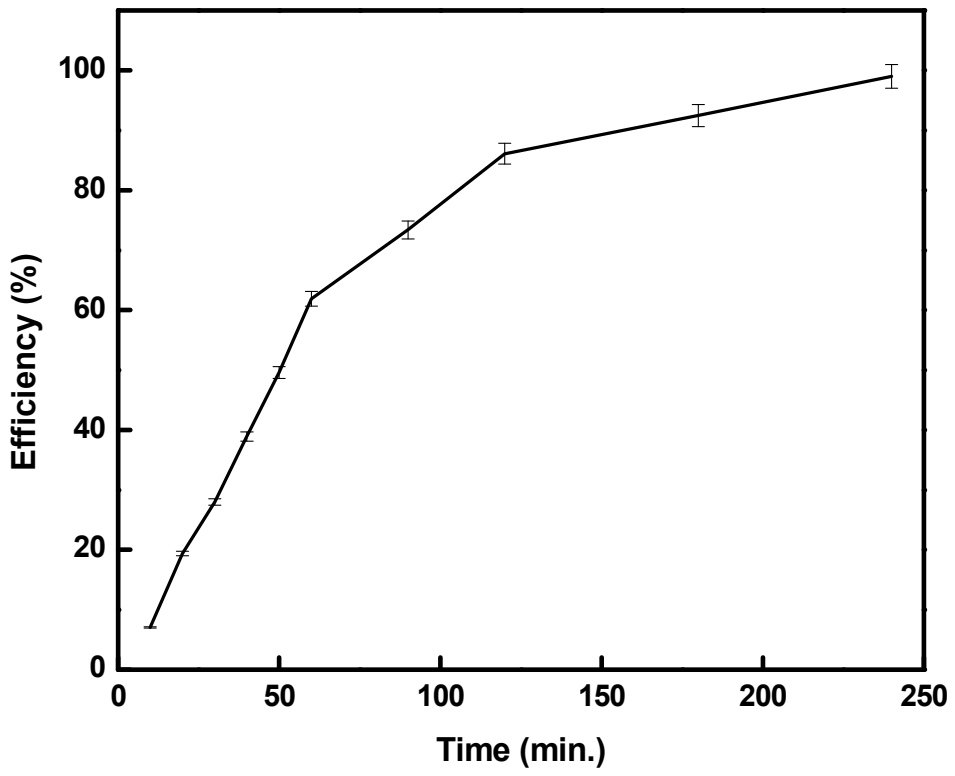

Fig. 9(c) Percentage efficiency of photodegradation of Rhodamine B (RhB) dye with time.

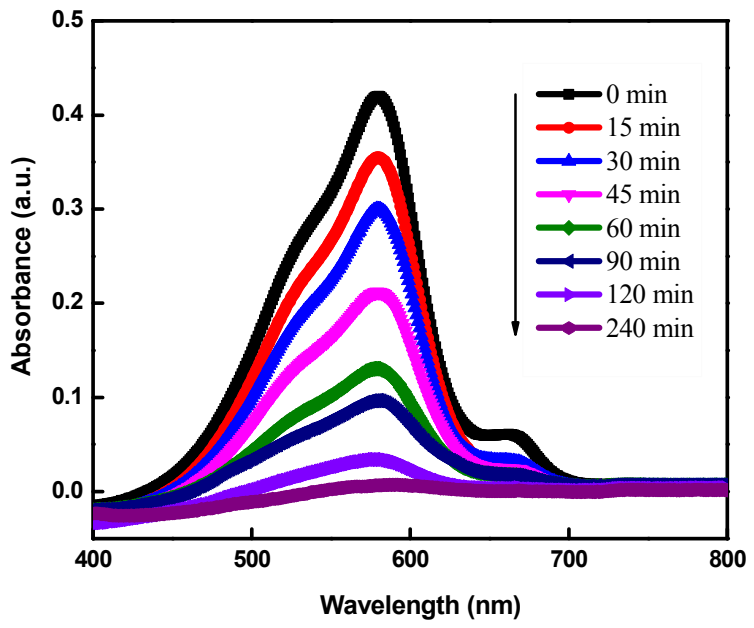

Fig. 10(a) Photocatalytic degradation of Methyl violet 6B (MV6B) dye by solar irradiation using synthesized SnO_2 nanopaticles (S1) as catalyst.

543

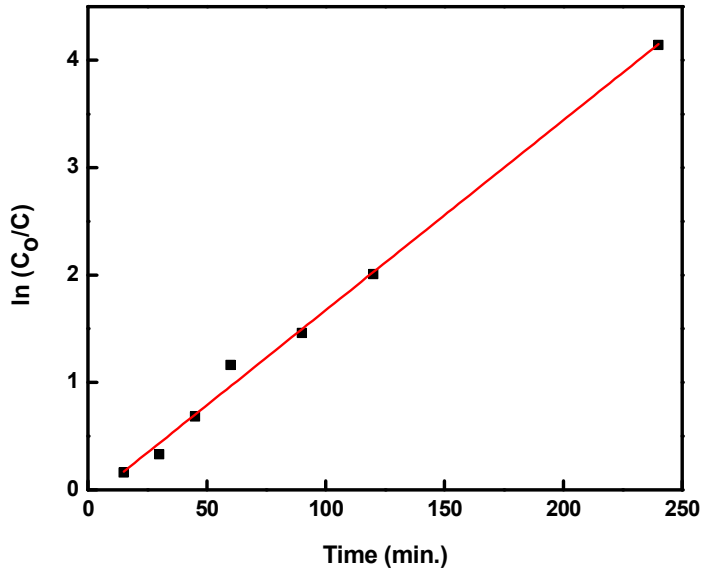

Fig. 10(b) Plot of $\ln(C_o/C)$ versus irradiation time for photodegradation of Methyl violet 6B dye (MV6B) using synthesized SnO_2 nanoparticles.

544

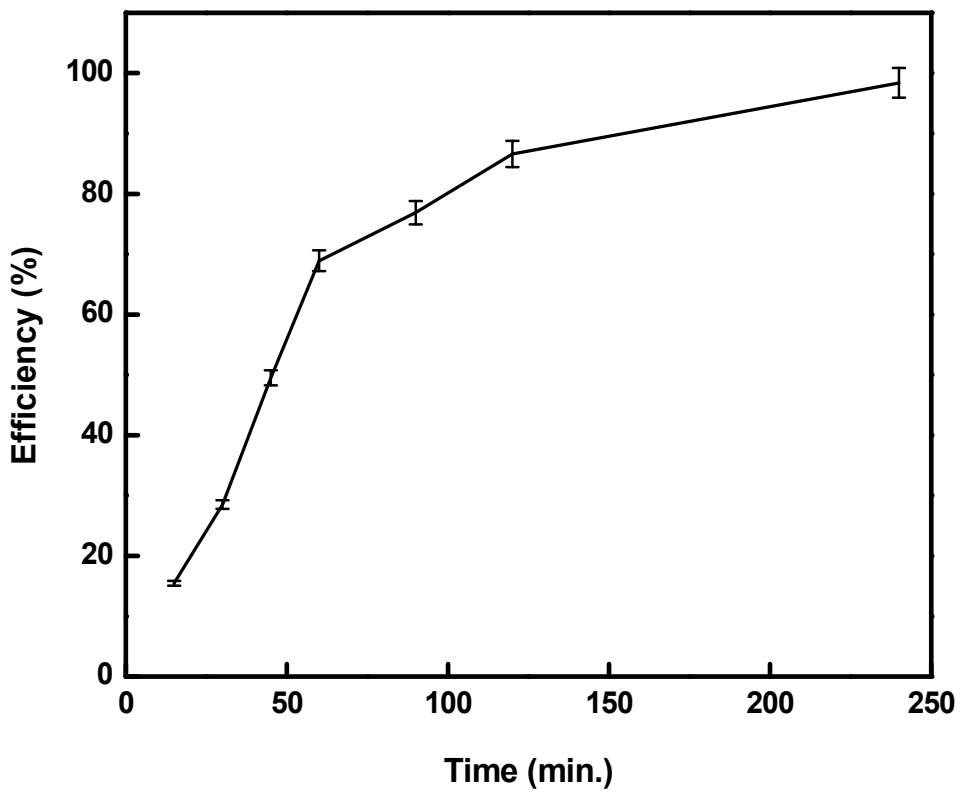

Fig. 10(c) Percentage efficiency of photodegradation of methyl violet 6B (MV6B) dye with time.

Table 1. Assignment of FT-IR bands of synthesized tin oxide nanoparticles

SnO_2 nanoparticles	FT- IR bands (cm^{-1})					
	ν_{O-H}	ν_{N-H}	ν_{C-H}	ν_{H2O} (def.)	ν_{C-O}	$\nu_{Sn-O-Sn}$
S1	3439	-	-	1629	-	610
S2	3442	3062	2919 (asym.), 2850 (sym.)	1629	-	600
S3	3439	-	2942 (asym.), 2876 (sym.)	1619	1248 (asym.), 1114 (sym.)	610

Table 2. Summary of results obtained from FT-IR, XRD, TEM and UV-visible spectroscopy for the synthesized SnO_2 nanoparticles (S1, S2 and S3)

SnO_2 NPs	Precursor	Surfactant	FT-IR bands (cm^{-1})	XRD (Average crystallite size, nm)	TEM (Average particle size, nm)	Morphology	Band gap energy (eV)
S1	$SnCl_2$+Urea	-	3439 cm^{-1} (ν_{O-H} str.), 1629 cm^{-1} (ν_{H2O} def.), 610 cm^{-1} ($\nu_{Sn-O-Sn}$ str.)	4.2	4.0	Spherical (A clock-like structure obtained in the domain of spherical SnO_2 nanoparticles)	4.30
S2	$SnCl_2$+Urea	CPC (cationic surfactant)	3442 cm^{-1} (ν_{O-H} str.), 3062 cm^{-1} (ν_{N-H} str.), 2919 cm^{-1} (ν_{C-H} asym. str.), 2850 cm^{-1} (ν_{C-H} sym. str.), 1629 cm^{-1} (ν_{H2O} def.), 600 cm^{-1} ($\nu_{Sn-O-Sn}$ str.)	4.8	4.5	Spherical	4.25
S3	$SnCl_2$+Urea	Triton X-100 (non-ionic surfactant)	3439 cm^{-1} (ν_{O-H} str.), 2942 cm^{-1} (ν_{C-H} asym. str.), 2876 cm^{-1} (ν_{C-H} sym. str.), 1619 cm^{-1} (ν_{H2O} def.), 1248 (ν_{O-H} asym. str.), 1114 (ν_{O-H} sym. str.), 610 cm^{-1} ($\nu_{Sn-O-Sn}$ str.)	6.0	5.8	Spherical	4.15